

Copyright © 1985, by the author(s).
All rights reserved.

Permission to make digital or hard copies of all or part of this work for personal or classroom use is granted without fee provided that copies are not made or distributed for profit or commercial advantage and that copies bear this notice and the full citation on the first page. To copy otherwise, to republish, to post on servers or to redistribute to lists, requires prior specific permission.

CANONICAL PIECEWISE-LINEAR MODELING

by

L. O. Chua and A.-C. Deng

Memorandum No. UCB/ERL M85/35

26 April 1985

ELECTRONICS RESEARCH LABORATORY

College of Engineering
University of California, Berkeley
94720

Canonical Piecewise-Linear Modeling†

Leon O. Chua and An-Chang Deng††

ABSTRACT

To take advantage of the remarkable computational efficiency of the canonical piecewise-linear approach for dc nonlinear electronic circuit analysis, the devices must be modeled by a canonical piecewise-linear model. This paper presents a unified parameter optimization algorithm for constructing such models. This algorithm is then applied to derive prototype canonical piecewise-linear models of pn junction diodes, bipolar transistors, MOSFETs, and GaAs FETs.

The canonical piecewise-linear model can be regarded as a *universal* model since its form remains unchanged for all devices. Only the coefficients differ from one device to another.

For large-scale circuits, the canonical piecewise-linear representation has a decisive advantage over other representations in regard to the number of memory locations needed to specify the equations.

† This work is supported by the Semiconductor Research Corporation under Grant SRC 82-11-008.

†† The authors are with the Department of Electrical Engineering and Computer Sciences and Electronics Research Laboratory, University of California, Berkeley, CA 94720.

1. Introduction

Device modeling is presently the weak link in computer-aided design. Without a good model for each electronic device in a circuit, no computer simulation would be meaningful. A good model always involves some compromise between simplicity and reality.

Modern electronic devices, especially those with submicron dimensions or operating at microwave frequencies, often exhibit strong nonlinearity and complicated dynamical phenomena. Consequently, circuit models for these devices are either presently unavailable, or are computationally so inefficient as to preclude their use in practical circuit simulation of large-scale circuits.

Several "*black box*" approaches (e.g., table lookup[1], spline function approximation[2,3]) have recently been used to derive simpler models so that they can be implemented efficiently in a circuit simulator. The table lookup method suffers the drawback of a huge memory space requirement for storing the device data. The higher-order spline function, though more general and can be made arbitrarily accurate, is made of higher-degree polynomials and is therefore still computationally inefficient especially for large-scale circuits. In this paper, we use canonical piecewise-linear functions[4] to model the nonlinear dc characteristics of practical electronic devices. The main advantage of this approach is that the resulting circuit equations to be solved by a circuit simulator will always possess the highly desirable canonical piecewise-linear form[9]. Such equations can be solved very efficiently, often at a tiny fraction of time needed by the other models. Since a piecewise-linear function may be considered as a first-order spline function in some applications, our model can not compete in the accuracy attainable with higher-degree spline functions. However, the remarkable saving in computation time often more than justifies the loss of some accuracy. Our experience has shown that the accuracy attainable using the canonical piecewise-linear models is satisfactory in most applications.

There is a significant difference between a *conventional* piecewise-linear model[5-8] and a *canonical* piecewise-linear model. The conventional piecewise-linear approximation consists of two major steps : (1) simplicial subdivision of the domain space; (2) interpolation of a piecewise-linear function on the subdivided domain. This approach suffers the drawback that the number of subdivided regions for a typical device is fairly large in order to obtain acceptable accuracy. Consequently, the total number of piecewise-linear regions in typical large-scale circuits becomes too large in both memory space and computation time for practical implementation. Our canonical piecewise-linear approach is entirely different

:

Starting from the measurement of the terminal v-i characteristic of the device, we fit these measured data into a compact global piecewise-linear representation called a *canonical piecewise-linear function*

$$f(\mathbf{x}) = \mathbf{a} + \mathbf{B}\mathbf{x} + \sum_{i=1}^{\sigma} \mathbf{c}_i | \langle \alpha_i, \mathbf{x} \rangle - \beta_i | \quad (1.1)$$

where \mathbf{a} , \mathbf{x} , \mathbf{c}_i , and α_i are n -dimensional vectors, \mathbf{B} is an $n \times n$ matrix, β_i is a scalar, and " \langle , \rangle " denotes the inner product of two vectors. Because no redundant data is stored, this approach greatly reduces the memory space required for the storage of the device parameters. Moreover, the special structure of the associated canonical piecewise-linear equation allows us to develop highly efficient algorithm for solving these equations[9-11]. In fact, it is the remarkable computational efficiency of the canonical piecewise-linear approach that motivates our development of canonical piecewise-linear models in this paper.

Using the optimization procedures derived in the following sections, we choose a set of optimal parameters \mathbf{a} , \mathbf{B} , \mathbf{c}_i , α_i , β_i for a given σ (i.e., the number of boundaries in the domain space), such that the approximation error is minimized. In this way, the internal physical phenomena of the device is not required as long as the terminal voltage and current can be accurately measured. In Section 2, we develop the parameter optimization algorithm for canonical piecewise-linear models of *2-terminal* devices. We then apply this algorithm to construct several canonical piecewise-linear models with increasing accuracy for a typical pn junction diode. This algorithm is extended to *3-terminal* devices in Section 3 and applied to three important 3-terminal devices; namely, bipolar transistors, MOSFETs (fixed bias for the substrate) and GaAs FETs. The canonical piecewise-linear models for these devices are validated by comparing the DP and TC characteristics of typical circuits with those derived from SPICE. In all cases, acceptable accuracy is obtained at a small fraction of computation time. The optimization algorithm developed in Sections 2 and 3 is extended in Section 4 to include multi-terminal and multi-port devices (e.g., op amps and gates). We also show that *parallel processing* can be applied to speed up our parameter optimization process. In the concluding Section 5, we compare the storage requirement of various methods for representing a high-dimensional function and show that among all known representations, the canonical piecewise-linear approach possesses the most economic storage especially for large-scale circuits.

2. Canonical Piecewise-Linear Modeling for 2-terminal Devices

Let x denote the terminal voltage (resp.; current) of a 2-terminal voltage-controlled (resp.; current-controlled) device; and let y denote its associated terminal current (resp.; voltage). Assume the set of data points $(x^{(l)}, y^{(l)})$, $l=1,2,\dots,N$ is obtained either by measuring the terminal v-i characteristic or by numerical computations from the equations which describe the physical phenomena of the device (e.g., 2-dimensional solution of the associated nonlinear partial differential equations). We want to find an optimal canonical piecewise-linear representation

$$y = a + bx + \sum_{i=1}^{\sigma} c_i |x - \beta_i| \quad (2.1)$$

for the v-i characteristic of the 2-terminal device such that Eq.(2.1) fits the measured data points as closely as possible. In other words, we want to find a set of optimal parameters $\{a, b, c_1, c_2, \dots, c_{\sigma}, \beta_1, \beta_2, \dots, \beta_{\sigma}\}$ such that the approximation error

$$E(\mathbf{z}_1, \mathbf{z}_2) \equiv \sum_{l=1}^N \left[w^{(l)} (a + bx^{(l)} + \sum_{i=1}^{\sigma} c_i |x^{(l)} - \beta_i| - y^{(l)})^2 \right] \quad (2.2)$$

is minimized, where

$$\mathbf{z}_1 \equiv [a \ b \ c_1 \ c_2 \ \dots \ c_{\sigma}]^T \quad (2.3)$$

$$\mathbf{z}_2 \equiv [\beta_1 \ \beta_2 \ \dots \ \beta_{\sigma}]^T \quad (2.4)$$

and $w^{(l)}$ for $l=1,2,\dots,N$, is the weighting factor for each data point.

We first assume that the location of each breakpoint is fixed at $\mathbf{z}_2 = \hat{\mathbf{z}}_2$, then the approximation error $E(\mathbf{z}_1, \hat{\mathbf{z}}_2)$ is a *quadratic* function of \mathbf{z}_1 and the minimum can be easily found by solving the linear equation

$$\frac{\partial E(\mathbf{z}_1, \hat{\mathbf{z}}_2)}{\partial \mathbf{z}_1} = 2 \mathbf{A} \mathbf{W} \mathbf{r} = 0 \quad (2.5)$$

where

$$\mathbf{A} = \begin{bmatrix} 1 & 1 & \dots & 1 \\ x^{(1)} & x^{(2)} & \dots & x^{(N)} \\ u_1^{(1)} & u_1^{(2)} & \dots & u_1^{(N)} \\ u_2^{(1)} & u_2^{(2)} & \dots & u_2^{(N)} \\ \vdots & \vdots & \ddots & \vdots \\ u_{\sigma}^{(1)} & u_{\sigma}^{(2)} & \dots & u_{\sigma}^{(N)} \end{bmatrix}, \quad \mathbf{r} = \begin{bmatrix} r^{(1)} \\ r^{(2)} \\ \vdots \\ r^{(N)} \end{bmatrix} \quad (2.6)$$

and

$$\mathbf{W} = \text{diag.} (w^{(1)}, w^{(2)}, \dots, w^{(N)}) \quad (2.7)$$

$$r^{(l)} = a + bx^{(l)} + \sum_{i=1}^{\sigma} c_i |x^{(l)} - \beta_i| - y^{(l)} \quad (2.8)$$

$$u_i^{(l)} = |x^{(l)} - \beta_i| \quad (2.9)$$

Since

$$\mathbf{r} = \mathbf{A}^T \mathbf{z}_1 - \mathbf{y} \quad (2.10)$$

where

$$\mathbf{y} = \left[y^{(1)} \ y^{(2)} \ \dots \ y^{(N)} \right]^T \quad (2.11)$$

Eq.(2.5) can be further reduced to

$$\mathbf{A}\mathbf{W}^{1/2}\mathbf{W}^{1/2}\mathbf{A}^T \mathbf{z}_1 - \mathbf{A}\mathbf{W}\mathbf{y} = 0 \quad (2.12)$$

where

$$\mathbf{W}^{1/2} \equiv \text{diag.} (\sqrt{w^{(1)}}, \sqrt{w^{(2)}}, \dots, \sqrt{w^{(N)}}) \quad (2.13)$$

Since the matrix $(\mathbf{A}\mathbf{W}^{1/2})(\mathbf{A}\mathbf{W}^{1/2})^T$ is symmetric, Eq.(2.12) can be solved by the more efficient Cholsky algorithm[12]. The solution $\mathbf{z}_1 = \mathbf{z}_1^*$ gives the optimal parameters for the fixed partition $\mathbf{z}_2 = \hat{\mathbf{z}}_2$. Clearly, different partitions would give rise to different optimal parameters and our goal is to choose an optimal partition boundaries $\mathbf{z}_2 = \mathbf{z}_2^*$. Let $\mathbf{z}_1 = \mathbf{z}_1^*(\mathbf{z}_2)$ be the optimal parameters for a particular partition boundaries \mathbf{z}_2 . Our problem is to find \mathbf{z}_2^* such that

$$E(\mathbf{z}_1^*(\mathbf{z}_2^*), \mathbf{z}_2^*) = \text{Min} \left\{ E(\mathbf{z}_1^*(\mathbf{z}_2), \mathbf{z}_2) \mid \mathbf{z}_2 \in R^\sigma \right\} \quad (2.14)$$

Define

$$\mathbf{g} = \frac{\partial E(\mathbf{z}_1, \mathbf{z}_2)}{\partial \mathbf{z}_2} = 2 \mathbf{K}\mathbf{G}\mathbf{W}\mathbf{r} \quad (2.15)$$

$$\mathbf{Y} = \frac{\partial \mathbf{g}}{\partial \mathbf{z}_2} = 2 \left[\mathbf{K} \left(\frac{\partial \mathbf{G}}{\partial \mathbf{z}_2} \right) \mathbf{W}\mathbf{r} + \mathbf{K}\mathbf{G}\mathbf{W}\mathbf{G}^T \mathbf{K}^T \right] \quad (2.16)$$

where

$$\mathbf{K} = \text{diag.} (c_1, c_2, \dots, c_\sigma) \quad (2.17)$$

$$\mathbf{G} = \begin{bmatrix} p_1^{(1)} & p_1^{(2)} & \dots & p_1^{(N)} \\ p_2^{(1)} & p_2^{(2)} & \dots & p_2^{(N)} \\ \vdots & \vdots & \vdots & \vdots \\ p_\sigma^{(1)} & p_\sigma^{(2)} & \dots & p_\sigma^{(N)} \end{bmatrix} \quad (2.18)$$

and

$$p_i^{(l)} = - \operatorname{sgn} (x^{(l)} - \beta_i) \quad (2.19)$$

where $\operatorname{sgn} (x) = 1$ (resp.; $\operatorname{sgn} (x) = -1$) if $x \geq 0$ (resp.; $x < 0$). Note that each element in the Hessian matrix $\frac{\partial \mathbf{G}}{\partial \mathbf{z}_2}$ is a first order generalized function which vanishes when no data point coincides with any of the breakpoints, i.e., when $x^{(l)} \neq \beta_i$ for $l=1,2,\dots,N$, and $i=1,2,\dots,\sigma$. Hence

$$\mathbf{Y} = 2 \mathbf{K} \mathbf{G} \mathbf{W} \mathbf{G}^T \mathbf{K}^T \quad (2.20)$$

almost everywhere.

Since $\mathbf{g} = \nabla_{\mathbf{z}_2} E$, $-\mathbf{g}$ specifies the steepest descent direction for E , i.e., the greatest initial rate of decrease in E . In practice, we do not use $-\mathbf{g}$ as the direction for our line search due to its slow convergence rate since no account is taken of the second order derivative of E w.r.t. \mathbf{z}_2 which, in this case, can be easily evaluated by using Eq.(2.20). Instead, we will perform a line search along the direction of

$$\mathbf{s} = -\mathbf{Y}^{-1} \mathbf{g} \quad (2.21)$$

which is guaranteed to be in the descent direction since \mathbf{Y} is positive definite. Let

$$\mathbf{g}^{(k)} = \mathbf{g} \big|_{\mathbf{z} = \mathbf{z}^{(k)}} \quad (2.22)$$

$$\mathbf{Y}^{(k)} = \mathbf{Y} \big|_{\mathbf{z} = \mathbf{z}^{(k)}} \quad (2.23)$$

$$\mathbf{s}^{(k)} = \mathbf{s} \big|_{\mathbf{z} = \mathbf{z}^{(k)}} \quad (2.24)$$

where

$$\mathbf{z}^{(k)} = \begin{bmatrix} \mathbf{z}_1^{(k)} \\ \mathbf{z}_2^{(k)} \end{bmatrix} \quad (2.25)$$

We start from an initial partition $\mathbf{z}_2 = \mathbf{z}_2^{(k)}$ for $k=0$, and solve Eq.(2.12) to obtain $\mathbf{z}_1^* (\mathbf{z}_2^{(k)})$. We then perform a line search along the direction $\mathbf{s}^{(k)}$ to find $\alpha^{(k)}$ such that

$$\begin{aligned} & E (\mathbf{z}_1^* (\mathbf{z}_2^{(k)} + \alpha^{(k)} \mathbf{s}^{(k)}), \mathbf{z}_2^{(k)} + \alpha^{(k)} \mathbf{s}^{(k)}) \\ & = \operatorname{Min} \left\{ E (\mathbf{z}_1^* (\mathbf{z}_2^{(k)} + \alpha \mathbf{s}^{(k)}), \mathbf{z}_2^{(k)} + \alpha \mathbf{s}^{(k)}) \mid \alpha \geq 0 \right\} \end{aligned} \quad (2.26)$$

Let

$$\mathbf{z}_2^{(k+1)} = \mathbf{z}_2^{(k)} + \alpha^{(k)} \mathbf{s}^{(k)} \quad (2.27)$$

and increment k by one to continue the iteration for minimizing E .

The above iteration procedures will reduce the approximation error E for each iteration and hence must approach a local minimum of E . Unfortunately, there generally exist more than one local minima as shown in the following Example 1, and hence it is not guaranteed that the parameters obtained by our iteration algorithm will lead to a global minimal approximation error. This local convergence phenomenon is typical of all general purpose optimization techniques.

Example 1 :

Figure 1(a) shows 15 data points located in the interval $[0,14]$ which are to be approximated by a two-segment (one breakpoint) piecewise-linear function. For each breakpoint location, we find the corresponding optimal canonical piecewise-linear representation by solving Eq.(2.12) and estimating the approximation error by Eq.(2.2) with a uniform weighting factor for each data point. The minimal approximation error E as a function of the breakpoint location β is shown in Fig.1(b), which shows that $\frac{\partial E}{\partial \beta}=0$ for $\beta=4.65, 6.75, 11.68, 0 \leq \beta < 1$, and $13 < \beta \leq 14$. However, the approximation error corresponding to the breakpoint in these locations is only locally minimal. The global minimum is located at $\beta=8$ where $\frac{\partial E}{\partial \beta}$ is discontinuous and is nonzero either from the left or the right limit of the point.

Example 1 shows that E has discontinuous derivative where the breakpoint β in this case coincides with a data point. This observation suggests the possibility that a local minimum may occur at the location of a data point $x^{(i)}$, if $\frac{\partial E}{\partial \beta} \Big|_{\beta = x^{(i)-}} < 0$ and $\frac{\partial E}{\partial \beta} \Big|_{\beta = x^{(i)+}} > 0$. It follows from this observation that it is impractical to search for a global minimum by searching for a critical point with $\frac{\partial E}{\partial \beta}=0$ since the derivative of E w.r.t. β is only piecewise continuous and E generally has multiple critical points. Hence, with the current state of the art in optimization techniques[13,14], searching for globally optimal canonical piecewise-linear model is presently not feasible in general.

Our strategy for finding the optimal breakpoints \mathbf{z}_2 is to combine the iteration procedures with a grid search. We start from an initial set of breakpoints and apply the above iteration procedure to minimize the approximation error. We then repeat this procedure with a new set of breakpoints chosen with a different spacing from the previous sets in order not to converge to the same local minimum. Finally, we compare all the local minima and choose the optimal

canonical piecewise-linear representation which has the smallest approximation error. Our experience shows that this strategy gives good results even though it is impossible to guarantee that we have indeed arrived at a global optimal solution.

Example 2 :

Assume there are 100 data points for a pn junction diode which are uniformly spaced between the interval $0.4 \leq x \leq 0.7$. For simplicity, let us obtain these data points from the standard pn junction law

$$i = I_s (e^{v/V_T} - 1) \quad (2.28)$$

where $I_s = 10^{-14}$ A and $V_T = 26$ mV. Following the above algorithm, we obtain the following optimal 2-segment canonical piecewise-linear model

$$i = a + bv + c_1 |v - \beta_1| \quad (2.29)$$

where $a = -2.351 \times 10^{-2}$, $b = 3.662 \times 10^{-2}$, $c_1 = 3.533 \times 10^{-2}$, and $\beta_1 = 0.648$ for this pn junction diode with an error $E = 1.05 \times 10^{-6}$.

As shown in the dashed curve of Fig.2, the canonical piecewise-linear diode model Eq.(2.29) obtained with a uniform weighting over the voltage range [0.4,0.7] has a serious defect : the error grows monotonically in the reversed biased region, which incidentally is outside of the range [0.4,0.7] of our data points. One way to improve our model is of course to enlarge our domain and take more data points. However, the computation time for optimization greatly increases with the number of data points. For the pn junction diode, however, the data points for $v < 0.4$ can be approximated by zero current in most applications. Hence, in this case, we need only to add one extra breakpoint β_0 to the model Eq.(2.29) such that the current is identically zero for all $v < \beta_0$. This new breakpoint can be physically interpreted as the *cut-in voltage* of the pn junction diode. Since the model in Eq.(2.29) realistically describes the diode characteristic in region $0.5 \leq v \leq 0.7$, we choose β_0 at the intersection of the v -axis and the piecewise-linear function described by Eq.(2.29), namely, $v = 0.481$. Hence, we simply introduce a new horizontal segment ($i = 0$) for $v \leq 0.481$. The resulting canonical piecewise-linear model is given by :

$$i = a + bv + c_0 |v - \beta_0| + c_1 |v - \beta_1| \quad (2.30)$$

where

$a = -2.320 \times 10^{-2}$, $b = 3.595 \times 10^{-2}$, $c_0 = 6.466 \times 10^{-4}$, $\beta_0 = 0.481$, $c_1 = 3.533 \times 10^{-2}$, and $\beta_1 = 0.648$, and is shown by the solid curve of Fig.2.

For future applications, several canonical piecewise-linear models with increasing accuracy (with more breakpoints) for the pn junction diode described by Eq.(2.28) are listed in Appendix A.

Remark : The saturation current I_s and the thermal voltage V_T in Eq.(2.28) may vary with different processing parameters in the fabrication of the pn junction diodes. Suppose that they differ from the nominal values $I_s=10^{-14}\text{A}$ and $V_T=26\text{mV}$ by a factor p and q respectively; i.e., the v-i characteristic follows the relation

$$i = pI_s (e^{v/qV_T} - 1) \quad (2.31)$$

then the corresponding optimal canonical piecewise-linear model can be easily extended by scaling the corresponding coefficients. More specifically, if Eq.(2.1) is the optimal canonical piecewise-linear model for the diode characterized by Eq.(2.28), then the optimal canonical piecewise-linear model for the diode described by Eq.(2.31) is simply given by

$$i = pa + \frac{p}{q}bv + \sum_{i=1}^{\sigma} \frac{p}{q}c_i |v - q\beta_i| \quad (2.32)$$

Summary : canonical piecewise-linear pn junction diode modeling algorithm :

A. Optimization

Step 0. Choose an initial set of breakpoints $\mathbf{z}_2^{(k)}$; $k=0$.

Step 1. Solve Eq.(2.12) for \mathbf{z}_1^* ($\mathbf{z}_2^{(k)}$).

Step 2. Find the line search direction $\mathbf{s}^{(k)}$ by Eqs.(2.15)-(2.21).

Step 3. Perform the line search along $\mathbf{s}^{(k)}$ to find $\alpha^{(k)}$ for the minimization problem of Eq.(2.26).

Step 4. Increment k to $k+1$.

Step 5. If $\|\mathbf{z}_2^{(k)} - \mathbf{z}_2^{(k-1)}\| < \epsilon$ (a constant specified by the user) then stop; else go to Step 1.

B. Refinement

Given Eq.(2.1) with parameters calculated from Steps 0-5, we can add one horizontal segment to the left of $v = \beta_0$ as in the preceding example and derive the following refined model :

$$i = a' + b'v + \sum_{i=0}^{\sigma} c_i |v - \beta_i| \quad (2.33)$$

where

$$\begin{aligned}
 c_0 &= \frac{1}{2} \left(b - \sum_{i=1}^{\sigma} c_i \right) \\
 \beta_0 &= \frac{a + \sum_{i=1}^{\sigma} c_i \beta_i}{\sum_{i=1}^{\sigma} c_i - b} \\
 b' &= b - c_0 \\
 a' &= a + \beta_0 c_0
 \end{aligned} \tag{2.34}$$

3. Canonical Piecewise-Linear Modeling for 3-terminal Devices

We now extend the algorithm developed in Section 2 for 3-terminal and 2-port devices. Let the terminal behavior of the 3-terminal device be characterized by

$$y_1 = f_1(x_1, x_2) \tag{3.1a}$$

$$y_2 = f_2(x_1, x_2) \tag{3.1b}$$

where x_1 (resp.; x_2) is the voltage or current in port 1 (resp.; port 2), and y_1 is the current or voltage associated with x_1 . Similar definition applies to y_2 .

Assume the data points $(x_i^{(l)}, y_i^{(l)})$, $i=1,2$, and $l=1,2,\dots,N$ are available which are scattered over the x_1 - x_2 domain space. The problem for modeling 3-terminal (or 2-port) devices is equivalent to finding the 2-dimensional surfaces

$$y_1 = \hat{f}_1(x_1, x_2) \tag{3.2a}$$

$$y_2 = \hat{f}_2(x_1, x_2) \tag{3.2b}$$

which fit the data points as closely as possible. In this section, the functions \hat{f}_1 and \hat{f}_2 are assumed to be canonical piecewise-linear functions; namely

$$y_1 = \hat{f}_1(x_1, x_2) = a_1 + b_{11}x_1 + b_{12}x_2 + \sum_{i=1}^{\sigma} c_{1i} | \alpha_{i1}x_1 + \alpha_{i2}x_2 + \beta_i | \tag{3.3a}$$

$$y_2 = \hat{f}_2(x_1, x_2) = a_2 + b_{21}x_1 + b_{22}x_2 + \sum_{i=1}^{\sigma} c_{2i} | \alpha_{i1}x_1 + \alpha_{i2}x_2 + \beta_i | \tag{3.3b}$$

The straight lines

$$\alpha_{i1}x_1 + \alpha_{i2}x_2 + \beta_i = 0 \tag{3.4}$$

for $i=1,2,\dots,\sigma$ are partition boundaries in the x_1 - x_2 plane. If $\alpha_{i2} \neq 0$, we can eliminate one coefficient from Eq.(3.4) by rewriting it into the equivalent form

$$m_i x_1 - x_2 + t_i = 0 \quad (3.5)$$

$i = 1, 2, \dots, \sigma$. For large σ , this will save a considerable amount of iteration procedures for finding the optimal partition boundaries. Although Eq.(3.5) excludes vertical boundary lines (i.e., when $\alpha_{i2} = 0$), such boundaries can be approximated by the straight line equation (3.5) with a large m_i and t_i . Hence, Eq.(3.3) can be simplified to

$$y_1 = \hat{f}_1(x_1, x_2) = a_1 + b_{11}x_1 + b_{12}x_2 + \sum_{i=1}^{\sigma} c_{1i} | m_i x_1 - x_2 + t_i | \quad (3.6a)$$

$$y_2 = \hat{f}_2(x_1, x_2) = a_2 + b_{21}x_1 + b_{22}x_2 + \sum_{i=1}^{\sigma} c_{2i} | m_i x_1 - x_2 + t_i | \quad (3.6b)$$

Let

$$\mathbf{z}_1 = \begin{bmatrix} a_1 \\ b_{11} \\ b_{12} \\ c_{11} \\ c_{12} \\ \vdots \\ c_{1\sigma} \end{bmatrix}, \quad \mathbf{z}_2 = \begin{bmatrix} a_2 \\ b_{21} \\ b_{22} \\ c_{21} \\ c_{22} \\ \vdots \\ c_{2\sigma} \end{bmatrix}, \quad \mathbf{z}_3 = \begin{bmatrix} m_1 \\ m_2 \\ \vdots \\ m_\sigma \\ t_1 \\ t_2 \\ \vdots \\ t_\sigma \end{bmatrix}, \quad \mathbf{z} = \begin{bmatrix} \mathbf{z}_1 \\ \mathbf{z}_2 \\ \mathbf{z}_3 \end{bmatrix} \quad (3.7)$$

then the approximation error between Eq.(3.6) and the data points is

$$E(\mathbf{z}) = \mathbf{r}_1^T \mathbf{W}_1 \mathbf{r}_1 + \mathbf{r}_2^T \mathbf{W}_2 \mathbf{r}_2 \quad (3.8)$$

where

$$\mathbf{r}_1 = \left[r_1^{(1)} \ r_1^{(2)} \ \dots \ r_1^{(N)} \right]^T \quad (3.9a)$$

$$\mathbf{r}_2 = \left[r_2^{(1)} \ r_2^{(2)} \ \dots \ r_2^{(N)} \right]^T \quad (3.9b)$$

$$r_1^{(l)} = a_1 + b_{11}x_1^{(l)} + b_{12}x_2^{(l)} + \sum_{i=1}^{\sigma} c_{1i} | m_i x_1^{(l)} - x_2^{(l)} + t_i | - y_1^{(l)} \quad (3.10a)$$

$$r_2^{(l)} = a_2 + b_{21}x_1^{(l)} + b_{22}x_2^{(l)} + \sum_{i=1}^{\sigma} c_{2i} | m_i x_1^{(l)} - x_2^{(l)} + t_i | - y_2^{(l)} \quad (3.10b)$$

and

$$\mathbf{W}_1 = \text{diag.} (w_1^{(1)}, w_1^{(2)}, \dots, w_1^{(N)}) \quad (3.11a)$$

$$\mathbf{W}_2 = \text{diag.} (w_2^{(1)}, w_2^{(2)}, \dots, w_2^{(N)}) \quad (3.11b)$$

are weighting factors for our error criterion.

Assume the location of each boundary line is fixed at $\mathbf{z}_3 = \hat{\mathbf{z}}_3$, then the approximation error $E(\mathbf{z}_1, \mathbf{z}_2, \hat{\mathbf{z}}_3)$ is again a *quadratic* function of \mathbf{z}_1 and \mathbf{z}_2 , and the minimum of E for the partition boundaries $\hat{\mathbf{z}}_3$ can be found by solving

$$\frac{\partial E}{\partial \mathbf{z}_1} = 2 \mathbf{A} \mathbf{W}_1 \mathbf{r}_1 = 0 \quad (3.12a)$$

$$\frac{\partial E}{\partial \mathbf{z}_2} = 2 \mathbf{A} \mathbf{W}_2 \mathbf{r}_2 = 0 \quad (3.12b)$$

where

$$\mathbf{A} = \begin{bmatrix} 1 & 1 & \dots & 1 \\ x_1^{(1)} & x_1^{(2)} & \dots & x_1^{(N)} \\ x_2^{(1)} & x_2^{(2)} & \dots & x_2^{(N)} \\ u_1^{(1)} & u_1^{(2)} & \dots & u_1^{(N)} \\ u_2^{(1)} & u_2^{(2)} & \dots & u_2^{(N)} \\ \vdots & \vdots & \ddots & \vdots \\ u_\sigma^{(1)} & u_\sigma^{(2)} & \dots & u_\sigma^{(N)} \end{bmatrix} \quad (3.13)$$

and

$$u_i^{(l)} = | m_i x_1^{(l)} - x_2^{(l)} + t_i | \quad (3.14)$$

Since

$$\mathbf{r}_1 = \mathbf{A}^T \mathbf{z}_1 - \mathbf{y}_1 \quad (3.15a)$$

$$\mathbf{r}_2 = \mathbf{A}^T \mathbf{z}_2 - \mathbf{y}_2 \quad (3.15b)$$

where

$$\mathbf{y}_1 = [y_1^{(1)} \ y_1^{(2)} \ \dots \ y_1^{(N)}]^T \quad (3.16a)$$

$$\mathbf{y}_2 = [y_2^{(1)} \ y_2^{(2)} \ \dots \ y_2^{(N)}]^T \quad (3.16b)$$

Equation (3.12) can be further reduced to

$$\mathbf{A} \mathbf{W}_1 \mathbf{A}^T \mathbf{z}_1 - \mathbf{A} \mathbf{W}_1 \mathbf{y}_1 = 0 \quad (3.17a)$$

$$\mathbf{A} \mathbf{W}_2 \mathbf{A}^T \mathbf{z}_2 - \mathbf{A} \mathbf{W}_2 \mathbf{y}_2 = 0 \quad (3.17b)$$

The optimal parameters for the fixed partition $\mathbf{z}_3 = \hat{\mathbf{z}}_3$ can be obtained by solving Eq.(3.17) and we denote them by $\mathbf{z}_1^*(\hat{\mathbf{z}}_3)$ and $\mathbf{z}_2^*(\hat{\mathbf{z}}_3)$. Hence, the minimal error for the fixed partition $\hat{\mathbf{z}}_3$ becomes

$$E(\mathbf{z}_1^*(\hat{\mathbf{z}}_3), \mathbf{z}_2^*(\hat{\mathbf{z}}_3), \hat{\mathbf{z}}_3) = \text{Min} \left\{ E(\mathbf{z}_1, \mathbf{z}_2, \mathbf{z}_3) \mid \mathbf{z}_3 = \hat{\mathbf{z}}_3 \right\} \quad (3.18)$$

and the optimal canonical piecewise-linear model is found by searching for the

optimal partition \mathbf{z}_3^* which will minimize the error in Eq.(3.8); namely

$$E(\mathbf{z}_1^*(\mathbf{z}_3^*), \mathbf{z}_2^*(\mathbf{z}_3^*), \mathbf{z}_3^*) = \text{Min} \left\{ E(\mathbf{z}_1, \mathbf{z}_2, \mathbf{z}_3) \right\} \quad (3.19)$$

We apply the same iteration procedure in Eqs.(2.15)-(2.27) for the 2-terminal case to search for an optimal partition except that \mathbf{g} and \mathbf{Y} which specify the direction

$$\mathbf{s} = -\mathbf{Y}^{-1}\mathbf{g} \quad (3.20)$$

for the line search are modified as follow :

$$\mathbf{g} = \frac{\partial E(\mathbf{z}_1, \mathbf{z}_2, \mathbf{z}_3)}{\partial \mathbf{z}_3} = 2 \mathbf{K}_1 \mathbf{G} \mathbf{W}_1 \mathbf{r}_1 + 2 \mathbf{K}_2 \mathbf{G} \mathbf{W}_2 \mathbf{r}_2 \quad (3.21)$$

$$\begin{aligned} \mathbf{Y} &= \frac{\partial \mathbf{g}}{\partial \mathbf{z}_3} \\ &= 2\mathbf{K}_1 \mathbf{G} \mathbf{W}_1 \mathbf{G}^T \mathbf{K}_1^T + 2\mathbf{K}_2 \mathbf{G} \mathbf{W}_2 \mathbf{G}^T \mathbf{K}_2^T + 2\mathbf{K}_1 \frac{\partial \mathbf{G}}{\partial \mathbf{z}_3} \mathbf{W}_1 \mathbf{r}_1 + 2\mathbf{K}_2 \frac{\partial \mathbf{G}}{\partial \mathbf{z}_3} \mathbf{W}_2 \mathbf{r}_2 \end{aligned} \quad (3.22)$$

where

$$\mathbf{K}_1 = \text{diag.} (c_{11}, c_{12}, \dots, c_{1\sigma}, c_{11}, c_{12}, \dots, c_{1\sigma}) \quad (3.23a)$$

$$\mathbf{K}_2 = \text{diag.} (c_{21}, c_{22}, \dots, c_{2\sigma}, c_{21}, c_{22}, \dots, c_{2\sigma}) \quad (3.23b)$$

$$\mathbf{G} = \begin{bmatrix} x_1^{(1)} p_1^{(1)} & x_1^{(2)} p_1^{(2)} & \dots & x_1^{(N)} p_1^{(N)} \\ x_1^{(1)} p_2^{(1)} & x_1^{(2)} p_2^{(2)} & \dots & x_1^{(N)} p_2^{(N)} \\ \vdots & \vdots & \ddots & \vdots \\ x_1^{(1)} p_\sigma^{(1)} & x_1^{(2)} p_\sigma^{(2)} & \dots & x_1^{(N)} p_\sigma^{(N)} \\ p_1^{(1)} & p_1^{(2)} & \dots & p_1^{(N)} \\ p_2^{(1)} & p_2^{(2)} & \dots & p_2^{(N)} \\ \vdots & \vdots & \ddots & \vdots \\ p_\sigma^{(1)} & p_\sigma^{(2)} & \dots & p_\sigma^{(N)} \end{bmatrix} \quad (3.24)$$

and

$$p_i^{(l)} = \text{sgn} (m_i x_1^{(l)} - x_2^{(l)} + t_i) \quad (3.25)$$

Just as in the 2-terminal case, \mathbf{Y} in Eq.(3.22) can be reduced to

$$\mathbf{Y} = 2 \mathbf{K}_1 \mathbf{G} \mathbf{W}_1 \mathbf{G}^T \mathbf{K}_1 + 2 \mathbf{K}_2 \mathbf{G} \mathbf{W}_2 \mathbf{G}^T \mathbf{K}_2 \quad (3.26)$$

if no data point is located on a boundary line.

We now apply the above algorithm to construct the canonical piecewise-linear models for three important 3-terminal devices; namely bipolar transistor,

MOSFET, and GaAs FET.

3.1. Canonical Piecewise-Linear Bipolar Transistor Model

Assume the npn bipolar transistor is connected in the common base configuration with $v_1=v_{BE}$, $v_2=v_{BC}$, $i_1=i_E$, and $i_2=i_C$ as shown in Fig.3. We take measurements from a set of uniformly-spaced grid points in a square region defined by $0.4 \leq v_1 \leq 0.7$ and $0.4 \leq v_2 \leq 0.7$, and assume the terminal behavior of the transistor follows the Ebers-Moll equation [15]; namely

$$i_1 = \frac{I_s}{\alpha_f} (e^{v_1/V_T} - 1) - I_s (e^{v_2/V_T} - 1) \quad (3.27a)$$

$$i_2 = \frac{I_s}{\alpha_r} (e^{v_2/V_T} - 1) - I_s (e^{v_1/V_T} - 1) \quad (3.27b)$$

with $I_s = 10^{-14} A$, $V_T = 26 mV$, $\alpha_f = 0.99$ and $\alpha_r = 0.5$. Following the above optimization procedure, we obtain the following canonical piecewise-linear model which optimally fits the data points with a uniform weighting factor in the error criterion defined by Eq.(3.8).

$$\begin{aligned} \begin{bmatrix} i_1 \\ i_2 \end{bmatrix} &= \begin{bmatrix} a_1 \\ a_2 \end{bmatrix} + \begin{bmatrix} b_{11} & b_{12} \\ b_{21} & b_{22} \end{bmatrix} \begin{bmatrix} v_1 \\ v_2 \end{bmatrix} + \begin{bmatrix} c_{11} \\ c_{21} \end{bmatrix} |m_1 v_1 - v_2 + t_1| \\ &+ \begin{bmatrix} c_{12} \\ c_{22} \end{bmatrix} |m_2 v_1 - v_2 + t_2| + \begin{bmatrix} c_{13} \\ c_{23} \end{bmatrix} |m_3 v_1 - v_2 + t_3| \quad (3.28) \end{aligned}$$

where

$$\begin{aligned} \begin{bmatrix} a_1 \\ a_2 \end{bmatrix} &= \begin{bmatrix} 5.8722 \times 10^{-3} \\ -3.2652 \times 10^{-2} \end{bmatrix}, \quad \begin{bmatrix} b_{11} \\ b_{21} \end{bmatrix} = \begin{bmatrix} 3.2392 \times 10^{-2} \\ -3.2067 \times 10^{-2} \end{bmatrix}, \quad \begin{bmatrix} b_{12} \\ b_{22} \end{bmatrix} = \begin{bmatrix} -4.0897 \times 10^{-2} \\ 8.1793 \times 10^{-2} \end{bmatrix} \\ \begin{bmatrix} c_{11} \\ c_{21} \end{bmatrix} &= \begin{bmatrix} 3.1095 \times 10^{-6} \\ -3.0784 \times 10^{-6} \end{bmatrix}, \quad \begin{bmatrix} c_{12} \\ c_{22} \end{bmatrix} = \begin{bmatrix} -9.9342 \times 10^{-3} \\ 1.9868 \times 10^{-2} \end{bmatrix}, \quad \begin{bmatrix} c_{13} \\ c_{23} \end{bmatrix} = \begin{bmatrix} -3.0471 \times 10^{-2} \\ 6.0943 \times 10^{-2} \end{bmatrix} \\ \begin{bmatrix} m_1 \\ m_2 \\ m_3 \end{bmatrix} &= \begin{bmatrix} 1.002 \times 10^4 \\ -1.4 \times 10^{-4} \\ 1.574 \times 10^{-6} \end{bmatrix}, \quad \begin{bmatrix} t_1 \\ t_2 \\ t_3 \end{bmatrix} = \begin{bmatrix} -6472 \\ 0.61714 \\ 0.66355 \end{bmatrix} \end{aligned}$$

This canonical piecewise-linear bipolar transistor model has the same defect as our earlier pn junction diode model : they give excessively large leakage currents. For example, when $v_1 = -1$ and $v_2 = 0$, Eq.(3.28) gives $i_1 = -1.588 mA$ and $i_2 = 1.346 mA$, both of which deviate from the small leakage current by a large approximation error. Note that there is nothing wrong with our optimization procedure since Eq.(3.28) is optimized only over the range $0.4 \leq v_1 \leq 0.7$ and $0.4 \leq v_2 \leq 0.7$.

One simple way to overcome this problem is to follow the idea in Section 2 which modifies the unrealistic diode model in Eq.(2.29) to that of Eq.(2.30) by adding one extra breakpoint. In the case of a 3-terminal device, this procedure corresponds to adding an extra *boundary line* such that both the emitter current and the collector current are forced to zero when the junction voltages are biased below the cut-in voltage determined by the new boundary line. By Eq.(3.28), the emitter current and the collector current are characterized respectively by

$$i_1 = 1.2348 \times 10^{-3} v_1 - 4.918 \times 10^{-4} v_2 - 3.5294 \times 10^{-4} \quad (3.29a)$$

$$i_2 = -1.2214 \times 10^{-3} v_1 + 9.82 \times 10^{-4} v_2 + 1.2466 \times 10^{-4} \quad (3.29b)$$

when both junctions are biased in the lower voltage region or are reverse biased where only a very small leakage current flows in the device. Hence, we simply choose the extra boundary line such that the current is zero in the lower voltage region while it remains unchanged in the other regions. However, if we follow the same procedure as in Section 2 which determines the extra breakpoint at the intersection of the zero current axis (v -axis) with the linear segment in the lower voltage region, we would obtain the following extra boundary lines for i_1 and i_2 , respectively :

$$1.2348 \times 10^{-3} v_1 - 4.918 \times 10^{-4} v_2 - 3.5294 \times 10^{-4} = 0 \quad (3.30a)$$

$$-1.2214 \times 10^{-3} v_1 + 9.82 \times 10^{-4} v_2 + 1.2466 \times 10^{-4} = 0 \quad (3.30b)$$

Unfortunately, Fig.4(a) shows that the addition of these two extra lines will not force the current to zero in the *whole* (shaded) lower voltage region. Since the extra boundary lines defined by Eqs.(3.30a) and (3.30b) fail to eliminate the excessive leakage current, a different pair of boundary lines must be chosen.

Let the emitter current and the collector current be characterized respectively by

$$i_1 = p_1 v_1 + q_1 v_2 + r_1 \quad (3.31a)$$

$$i_2 = p_2 v_1 + q_2 v_2 + r_2 \quad (3.31b)$$

in the lower voltage region of Eq.(3.28) when both junction voltages v_1 and v_2 are reverse-biased. Assume that the new boundary lines are located at $v_1 = E_1$ and $v_2 = E_2$ as shown in Fig.4(b), where E_1 and E_2 are to be chosen such that the currents in region I are still characterized by Eq.(3.31) but are zero in region IV. Note that the equations which specify the currents in region II (resp.; region III) is not a function of v_1 (resp.; v_2) because they are independent of the junction voltages when reverse-biased or biased below the cut-in voltage. Moreover, since our canonical piecewise-linear model is *continuous* , the linear equations

governing neighboring regions must be identical at their common boundaries. Consequently, the linear equation governing region II must have the form :

$$i_1 = q_1 v_2 + p_1 E_1 + r_1 \quad (3.32a)$$

$$i_2 = q_2 v_2 + p_2 E_1 + r_2 \quad (3.32b)$$

Note that i_1 and i_2 in Eq.(3.32) do not depend on v_1 and are identical to Eq.(3.31) when $v_1 = E_1$. Similarly, the linear equations governing region III must have the form :

$$i_1 = p_1 v_1 + q_1 E_2 + r_1 \quad (3.33a)$$

$$i_2 = p_2 v_1 + q_2 E_2 + r_2 \quad (3.33b)$$

Setting $i_1 = i_2 = 0$ in Eq.(3.32) and solving for E_2 , we obtain

$$\frac{p_1 E_1 + r_1}{q_1} = \frac{p_2 E_1 + r_2}{q_2} = -E_2 \quad (3.34)$$

Setting $i_1 = i_2 = 0$ in Eq.(3.33) and solving for E_1 , we obtain

$$\frac{q_1 E_2 + r_1}{p_1} = \frac{q_2 E_2 + r_2}{p_2} = -E_1 \quad (3.35)$$

The location of the new boundary lines can now be found by solving Eqs.(3.34) and (3.35) :

$$v_1 = E_1 = \frac{q_1 r_2 - q_2 r_1}{p_1 q_2 - p_2 q_1} \quad (3.36a)$$

$$v_2 = E_2 = \frac{p_1 r_2 - p_2 r_1}{p_2 q_1 - p_1 q_2} \quad (3.36b)$$

Substituting the numerical values of the parameters from Eq.(3.29) into Eq.(3.36), we obtain $E_1=0.4662$, $E_2=0.4529$. The canonical piecewise-linear model in Eq.(3.28) now assumes the form

$$\begin{aligned} \begin{bmatrix} i_1 \\ i_2 \end{bmatrix} &= \begin{bmatrix} a_1' \\ a_2' \end{bmatrix} + \begin{bmatrix} b_{11}' & b_{12}' \\ b_{21}' & b_{22}' \end{bmatrix} \begin{bmatrix} v_1 \\ v_2 \end{bmatrix} + \begin{bmatrix} d_{11} \\ d_{21} \end{bmatrix} |v_1 - E_1| + \begin{bmatrix} d_{12} \\ d_{22} \end{bmatrix} |v_2 - E_2| \\ &+ \begin{bmatrix} c_{11} \\ c_{21} \end{bmatrix} |m_1 v_1 - v_2 + t_1| + \begin{bmatrix} c_{12} \\ c_{22} \end{bmatrix} |m_2 v_1 - v_2 + t_2| \\ &+ \begin{bmatrix} c_{13} \\ c_{23} \end{bmatrix} |m_3 v_1 - v_2 + t_3| \end{aligned} \quad (3.37)$$

where

$$\begin{bmatrix} a_1' \\ a_2' \end{bmatrix} = \begin{bmatrix} 6.0482 \times 10^{-3} \\ -3.271 \times 10^{-2} \end{bmatrix}, \quad \begin{bmatrix} b_{11}' \\ b_{21}' \end{bmatrix} = \begin{bmatrix} 3.1775 \times 10^{-2} \\ -3.1456 \times 10^{-2} \end{bmatrix}, \quad \begin{bmatrix} b_{12}' \\ b_{22}' \end{bmatrix} = \begin{bmatrix} -4.065 \times 10^{-2} \\ 8.1302 \times 10^{-2} \end{bmatrix}$$

$$\begin{bmatrix} d_{11} \\ d_{21} \end{bmatrix} = \begin{bmatrix} 6.174 \times 10^{-4} \\ -6.107 \times 10^{-4} \end{bmatrix}, \quad \begin{bmatrix} d_{12} \\ d_{22} \end{bmatrix} = \begin{bmatrix} -2.459 \times 10^{-4} \\ 4.910 \times 10^{-4} \end{bmatrix}, \quad \begin{bmatrix} E_1 \\ E_2 \end{bmatrix} = \begin{bmatrix} 0.4662 \\ 0.4529 \end{bmatrix}$$

and other parameters (namely, $m_1, m_2, m_3, t_1, t_2, t_3, c_{11}, c_{21}, c_{12}, c_{22}, c_{13}$ and c_{23}) are the same as those in Eq.(3.28). As a check, note that $i_1 = i_2 = 0$ in Eq.(3.37) for all $v_1 \leq E_1$ and $v_2 \leq E_2$, as they should.

Remark : Since each boundary line in Eq.(3.37) is either identical to or close to a vertical line or horizontal line, we can approximate Eq.(3.37) by the following simplified canonical piecewise-linear model which possesses a *lattice structure* :

$$\begin{bmatrix} i_1 \\ i_2 \end{bmatrix} = \begin{bmatrix} a_{11}' \\ a_{21}' \end{bmatrix} + \begin{bmatrix} b_{11}' & b_{12}' \\ b_{21}' & b_{22}' \end{bmatrix} \begin{bmatrix} v_1 \\ v_2 \end{bmatrix} + \begin{bmatrix} d_{11} \\ d_{21} \end{bmatrix} |v_1 - E_1| + \begin{bmatrix} d_{12} \\ d_{22} \end{bmatrix} |v_2 - E_2| \\ + \begin{bmatrix} c_{11}' \\ c_{21}' \end{bmatrix} |v_1 - \beta_{11}| + \begin{bmatrix} c_{12} \\ c_{22} \end{bmatrix} |v_2 - \beta_{21}| + \begin{bmatrix} c_{13} \\ c_{23} \end{bmatrix} |v_2 - \beta_{22}| \quad (3.38)$$

where $c_{11}' = m_1 c_{11}, c_{21}' = m_1 c_{21}, \beta_{11} = -\frac{t_1}{m_1}, \beta_{21} = t_2, \beta_{22} = t_3$, and the other parameters remain unchanged. The simplified Eq.(3.38) is said to possess a *lattice structure* because each term within an absolute-value sign involves only *one* variable. Geometrically, this structure is equivalent to the property that boundaries are parallel to either v_1 or v_2 axis. Such models are highly desirable because the associated circuit equations can be solved with great computational efficiency[10,11].

For future applications, two canonical piecewise-linear bipolar transistor models optimized for different dynamic ranges are listed in Appendix B. Several graphical comparisons of the predicted emitter and collector currents between the Ebers-Moll model in Eq.(3.27) and the canonical piecewise-linear model in Eq.(B.1) (low voltage version) are given in Figs.5(a)-(e). Note the agreement is quite good in each case.

Example 3 :

The transistor circuit in Fig.6(a) is an odd-symmetric negative resistance device[16] which exhibits a negative slope in its driving-point characteristic as shown by the dashed curve in Fig.6(b). This characteristic is obtained by the recent algorithm described in [17] with each bipolar transistor characterized by Eq.(3.27). Using the canonical piecewise-linear model in Eq.(B.2) (higher voltage version) for each transistor, we efficiently trace the driving-point characteristic by the *Breakpoint Hopping Algorithm* [10] as shown by the solid curve of Fig.6(b). Observe from Fig.6(b) that both driving-point characteristics are virtually

identical in the region $|v_{in}| < 0.75$. Yet the solid curve is obtained at only an insignificant fraction of the time needed to trace the dotted curve. The discrepancy beyond 0.75V is expected since our model is optimized only for voltages less than 0.75V. If we add more boundary lines in the higher voltage region, then both curves in Fig.6(b) will be colse to each other even for higher input voltages.

3.2. Canonical Piecewise-Linear MOSFET Model

Assume the MOSFET is connected in the common source configuration with $v_1=v_{GS}$, $v_2=v_{DS}$, $i_1=i_G$, and $i_2=i_D$ as shown in Fig.7, where both v_1, v_2 are in *Volt*, and i_1, i_2 are in μA . The data points are uniformly spaced in a grid within a rectangular region defined by $0 \leq v_1 \leq 5$, and $0 \leq v_2 \leq 5$. We assume the data points follow the Shichman-Hodges model[18]; namely

$$i_1 = 0$$

$$i_2 = k [(v_1 - V_t)v_2 - 0.5v_2^2]$$

if $v_1 - V_t \geq v_2$; or

$$i_2 = 0.5k (v_1 - V_t)^2 [1 + \lambda(v_2 - v_1 + V_t)] \quad (3.39)$$

if $v_1 - V_t < v_2$, with $k = 50\mu A / V^2$, $V_t = 1 \text{ Volt}$, $\lambda = 0.02 V^{-1}$. Applying the above optimization algorithm with uniform weighting factor for each data point, we obtain the following canonical piecewise-linear model which optimally fits the data points with $N = 3$ boundary lines :

$$i_2 = a_2 + b_{21}v_1 + b_{22}v_2 + c_{21} | m_1v_1 - v_2 + t_1 | + c_{22} | m_2v_1 - v_2 + t_2 | + c_{23} | m_1v_1 - v_2 + t_3 | \quad (3.40)$$

where

$$a_2 = -61.167, b_{21} = 30.242, b_{22} = 72.7925$$

$$c_{21} = -49.718, c_{22} = -21.027, c_{23} = 2.0348$$

$$m_1 = 0.8175, m_2 = 1.0171, m_3 = -23.406$$

$$t_1 = -2.1052, t_2 = -1.4652, t_3 = 69$$

Just as in the preceding canonical piecewise-linear pn junction and bipolar transistor models, Eq.(3.40) predicts an excessive leakage current below the threshold voltage V_t . We can eliminate the leakage current by adding one extra boundary as before such that the current i_2 is forced to zero for $v_1 \leq V_t$ but remains unchanged elsewhere. By Eq.(3.40), the drain current in the lower voltage region

$(v_1 \leq V_t)$ is characterized by

$$i_2 = 44.647v_1 + 0.0252v_2 - 56.239 \quad (3.41)$$

Setting $i_2 = 0$ in Eq.(3.41) specifies the extra boundary line at

$$44.647v_1 + 0.0252v_2 - 56.239 = 0 \quad (3.42)$$

This new boundary line is very close to the vertical line $v_1=1.26$ and defines the threshold voltage V_t such that the drain current is identically zero in the region $v_1 \leq V_t$. By augmenting this new boundary line, we obtain the following improved canonical piecewise-linear MOSFET model :

$$\begin{aligned} i_2 = & a_2' + b_{21}' v_1 + b_{22}' v_2 + c_{20} | m_0 v_1 - v_2 + t_0 | + c_{21} | m_1 v_1 - v_2 + t_1 | \\ & + c_{22} | m_2 v_1 - v_2 + t_2 | + c_{23} | m_3 v_1 - v_2 + t_3 | \end{aligned} \quad (3.43)$$

where

$$\begin{aligned} a_2' = & -33.048, b_{21}' = 7.919, b_{22}' = 72.792 \\ c_{20} = & 0.0126, m_0 = -1771.7, t_0 = 2231.7 \end{aligned}$$

and the other parameters remain unchanged.

Two three-dimensional plots for the i_D surface over the $v_{GS}-v_{DS}$ plane are shown in Fig.8. The surface in Fig.8(a) is calculated from Eq.(3.39). The surface in Fig.8(b) is calculated from Eq.(3.43). The corresponding families of drain current characteristic are superimposed in Fig.8(c) where the solid curves are plotted from Eq.(3.43). Observe that the two models agree quite well except in the region when both v_{DS} and i_D are very small. This discrepancy is not surprising since Eq.(3.43) is obtained by optimizing the error with a uniform weighting factor. This deviation of the canonical piecewise-linear MOSFET model from the device characteristic in the small v_{DS} region will shift the computed v_{DS} voltage by approximately ± 0.2 Volt, and is of little concern in most applications. In those cases (e.g., dynamic memory circuits) where this deviation becomes objectionable, a different weighting factor in the error criterion is required. For example, choosing $w^{(l)} = 5$ for all data points with $v_2^{(l)} \leq 2$ and $w^{(l)} = 1$ for $v_2^{(l)} > 2$, we obtain the following canonical piecewise-linear MOSFET model

$$\begin{aligned} i_2 = & a_2 + b_{21}v_1 + b_{22}v_2 + c_{21} | m_1 v_1 - v_2 + t_1 | + c_{22} | m_2 v_1 - v_2 + t_2 | \\ & + c_{23} | m_3 v_1 - v_2 + t_3 | + c_{24} | m_4 v_1 - v_2 + t_4 | \end{aligned} \quad (3.44)$$

where

$$\begin{aligned} a_2 = & -12.405, b_{21} = 3.286, b_{22} = 71.493 \\ c_{21} = & 0.438, c_{22} = -54.407, c_{23} = -15.715, c_{24} = 1.809 \end{aligned}$$

$$m_1 = 37.738, m_2 = 0.6705, m_3 = 1.043, m_4 = -21.904$$

$$t_1 = 42.459, t_2 = -1.5385, t_3 = -1.3058, t_4 = 54.166$$

The resulting characteristics are shown in Figs.8(d) and 8(e). Observe the significant improvement in the small v_{DS} region.

Example 4 :

The circuit in Fig.9(a) is an NMOS depletion load inverter where the enhancement type driving transistor is characterized by the canonical piecewise-linear model in Eq.(3.43), and the depletion load transistor is characterized by the same canonical piecewise-linear equation but with the threshold voltage shifted by -3V; namely,

$$\begin{aligned} i_2 = & a_2 + b_{21}v_1 + b_{22}v_2 + c_{21} | m_1v_1 - v_2 + t_1 | + c_{22} | m_2v_1 - v_2 + t_2 | \\ & + c_{23} | m_3v_1 - v_2 + t_3 | + c_{24} | m_4v_1 - v_2 + t_4 | \end{aligned} \quad (3.45)$$

where

$$a_2 = -9.291, b_{21} = 7.919, b_{22} = 72.792$$

$$c_{21} = -49.718, c_{22} = -21.027, c_{23} = 2.035, c_{24} = 0.0126$$

$$m_1 = 0.8175, m_2 = 1.0171, m_3 = -23.406, m_4 = -1771.7$$

$$t_1 = 0.3473, t_2 = 1.586, t_3 = -1.217, t_4 = -3083.4$$

The $v_{out} - v_s - v_{in}$ transfer characteristic of this inverter circuit is easily calculated by the *Generalized Breakpoint Hopping Algorithm* [11] as shown in Fig.9(b) (solid curve). The superimposed dashed curve is obtained by SPICE where the driving enhancement transistor is characterized by Eq.(3.39) and the depletion load transistor is similarly characterized but with -3V shift in the threshold voltage. Observe that the two curves are very close to each other. Yet the solid curve is obtained at only a tiny fraction of time needed to calculate the dashed curve.

Example 5 :

The circuit in Fig.10(a) is a CMOS inverter circuit with the NMOS driving transistor characterized by Eq.(3.43) and the PMOS transistor similarly characterized except the voltage polarities and the current direction are reversed. The solid $v_{out} - v_s - v_{in}$ transfer characteristic shown in Fig.10(b) (obtained by the Generalized Breakpoint Hopping Algorithm) is very close to the dashed curve obtained by SPICE (with the transistors modeled by Eq.(3.39)).

3.3. Canonical Piecewise-Linear Model of GaAs FET

We now apply the same optimization algorithm to a third practical 3-terminal device; namely, the GaAs FET, which has become increasingly important in the development of microwave circuits and high-speed digital IC's due to its fast switching speed. In order to demonstrate the simplicity and accuracy of our canonical piecewise-linear model, the input data set for our optimization program is chosen from the same experimental data measured from an ion-implanted GaAs FET in a recent paper[19]. The computed optimal canonical piecewise-linear model for $\sigma=3$ is

$$i_2 = a_2 + b_{21}v_1 + b_{22}v_2 + c_{21} | m_1v_1 - v_2 + t_2 | + c_{22} | m_2v_1 - v_2 + t_2 | + c_{23} | m_3v_1 - v_2 + t_3 | \quad (3.46)$$

where $v_1=v_{GS}$ (Volt), $v_2=v_{DS}$ (Volt), $i_2=i_D$ (mA), and

$$\begin{aligned} a_2 &= 6.3645, \quad b_{21} = 2.4961, \quad b_{22} = 32.339 \\ c_{21} &= 0.6008, \quad c_{22} = 0.9819, \quad c_{23} = -29.507 \\ m_1 &= -19.594, \quad m_2 = -6.0736, \quad m_3 = 0.6473 \\ t_1 &= -44.551, \quad t_2 = -8.9962, \quad t_3 = 1.3738 \end{aligned}$$

Observe that this model requires only only 3 absolute-valued functions and 12 numerical coefficients. It is far simpler than the analytical model derived in [19] which involves 45 physical parameters and more than 40 equations which are necessary to account for the extremely complicated physical phenomena inside the device. Our canonical piecewise-linear model in Eq.(3.46) is so simple that it seems incredible that it could realistically mimic the terminal behavior of the device. However, as shown in Fig.11, the drain current calculated from Eq.(3.46) (solid line) matches the measured data fairly well, and in some regions of operation, it is even better than the analytical model (dashed line). This comparison clearly demonstrates the versatility of the canonical piecewise-linear modeling approach.

Summary : canonical piecewise-linear 3-terminal device modeling algorithm :

A. Optimization

- Step 0. Choose an initial set of boundary lines as $z_3^{(k)}$; $k=0$.
- Step 1. Solve Eq.(3.12) or Eq.(3.17) for $z_1^*(z_3^{(k)})$ and $z_2^*(z_3^{(k)})$.
- Step 2. Find the line search direction $s^{(k)}$ by Eqs.(3.20)-(3.26).

Step 3. Perform the line search along $\mathbf{s}^{(k)}$ to find $\alpha^{(k)}$ for the minimization problem of

$$\begin{aligned} & E(\mathbf{z}_1^*(\mathbf{z}_3^{(k)} + \alpha^{(k)}\mathbf{s}^{(k)}), \mathbf{z}_2^*(\mathbf{z}_3^{(k)} + \alpha^{(k)}\mathbf{s}^{(k)}), \mathbf{z}_3^{(k)} + \alpha^{(k)}\mathbf{s}^{(k)}) \\ &= \text{Min} \left\{ E(\mathbf{z}_1^*(\mathbf{z}_3^{(k)} + \alpha\mathbf{s}^{(k)}), \mathbf{z}_2^*(\mathbf{z}_3^{(k)} + \alpha\mathbf{s}^{(k)}), \mathbf{z}_3^{(k)} + \alpha\mathbf{s}^{(k)}) \mid \alpha \geq 0 \right\} \end{aligned} \quad (3.47)$$

Step 4. Increment k to $k+1$.

Step 5. If $\|\mathbf{z}_3^{(k)} - \mathbf{z}_3^{(k-1)}\| < \epsilon$ (a constant specified by the user) then stop; else go to Step 1.

B. Refinement

Given Eq.(3.6) with parameters calculated from Steps 0-5, we can improve the model accuracy in the subthreshold region as follows :

(1) Bipolar Transistor

$$\begin{aligned} i_1 &= a_1' + b_{11}' v_1 + b_{12}' v_2 + d_{11} |v_1 - E_1| + d_{12} |v_2 - E_2| \\ &\quad + \sum_{i=1}^{\sigma} c_{1i} |m_i v_1 - v_2 + t_i| \end{aligned} \quad (3.48a)$$

$$\begin{aligned} i_2 &= a_2' + b_{21}' v_1 + b_{22}' v_2 + d_{21} |v_1 - E_1| + d_{22} |v_2 - E_2| \\ &\quad + \sum_{i=1}^{\sigma} c_{2i} |m_i v_1 - v_2 + t_i| \end{aligned} \quad (3.48b)$$

where

$$\begin{aligned} E_1 &= \frac{q_1 r_2 - q_2 r_1}{p_1 q_2 - p_2 q_1}, \quad E_2 = \frac{p_1 r_2 - p_2 r_1}{p_2 q_1 - p_1 q_2} \\ d_{11} &= \frac{1}{2} p_1, \quad d_{12} = \frac{1}{2} q_1, \quad d_{21} = \frac{1}{2} p_2, \quad d_{22} = \frac{1}{2} q_2 \\ b_{11}' &= b_{11} - d_{11}, \quad b_{12}' = b_{12} - d_{12}, \quad b_{21}' = b_{21} - d_{21}, \quad b_{22}' = b_{22} - d_{22} \\ a_1' &= a_1 + d_{11} E_1 + d_{12} E_2, \quad a_2' = a_2 + d_{21} E_1 + d_{22} E_2 \end{aligned} \quad (3.49)$$

and

$$\begin{aligned} p_1 &= b_{11} + \sum_{i=1}^{\sigma} c_{1i} m_i \text{sgn}(t_i), \quad q_1 = b_{12} - \sum_{i=1}^{\sigma} c_{1i} \text{sgn}(t_i) \\ p_2 &= b_{21} + \sum_{i=1}^{\sigma} c_{2i} m_i \text{sgn}(t_i), \quad q_2 = b_{22} - \sum_{i=1}^{\sigma} c_{2i} \text{sgn}(t_i) \\ r_1 &= a_1 + \sum_{i=1}^{\sigma} c_{1i} |t_i|, \quad r_2 = a_2 + \sum_{i=1}^{\sigma} c_{2i} |t_i| \end{aligned} \quad (3.50)$$

(2) MOSFET

$$i_2 = a' + b_1' v_1 + b_2' v_2 + \sum_{i=0}^{\sigma} c_i | m_i v_1 - v_2 + t_i | \quad (3.51)$$

where

$$t_0 = -\frac{a + \sum_{i=1}^{\sigma} c_i | t_i |}{b_2 - \sum_{i=1}^{\sigma} c_i \operatorname{sgn}(t_i)}$$

$$c_0 = \frac{1}{2} [b_2 - \sum_{i=1}^{\sigma} c_i \operatorname{sgn}(t_i)] \operatorname{sgn}(t_0)$$

$$m_0 = -\frac{b_1 + \sum_{i=1}^{\sigma} c_i m_i \operatorname{sgn}(t_i)}{b_2 - \sum_{i=1}^{\sigma} c_i \operatorname{sgn}(t_i)}$$

$$a' = a + c_0 | t_0 |$$

$$b_1' = b_1 + c_0 m_0 \operatorname{sgn}(t_0)$$

$$b_2' = b_2 - c_0 \operatorname{sgn}(t_0) \quad (3.52)$$

4. Canonical Piecewise-Linear Modeling for Multi-Terminal and Multi-Port Devices

The algorithm developed in Sections 2 and 3 can be easily extended for modeling $(n+1)$ -terminal and n -port devices. Assume the terminal behavior of the device is described by a set of data points $(x_i^{(l)}, y_i^{(l)})$, $i=1,2,\dots,n$, and $l=1,2,\dots,N$, which are obtained either by measurement or by numerical solution of the physical equations governing the device, where $x_i^{(l)}$ and $y_i^{(l)}$ denote the voltage and current of the i -th port in the l -th data point

$$\mathbf{x}^{(l)} = [x_1^{(l)} \ x_2^{(l)} \ \dots \ x_n^{(l)}]^T \quad (4.1a)$$

$$\mathbf{y}^{(l)} = [y_1^{(l)} \ y_2^{(l)} \ \dots \ y_n^{(l)}]^T \quad (4.1b)$$

The points $\mathbf{x}^{(l)}$, $l=1,2,\dots,N$ are scattered over the \mathbf{x} -space and do not necessarily have a uniform distribution. In general, more data points must be measured in regions with sharp changing characteristic. These data points are used to fit the n -dimensional canonical piecewise-linear equation

$$\mathbf{y} = \mathbf{f}(\mathbf{x}) = \mathbf{a} + \mathbf{B}\mathbf{x} + \sum_{i=1}^{\sigma} c_i | \langle \alpha_i, \mathbf{x} \rangle - \beta_i | \quad (4.2)$$

such that the approximation error

$$E = \sum_{l=1}^N \left[\mathbf{y}^{(l)} - \mathbf{f}(\mathbf{x}^{(l)}) \right]^T \mathbf{W}^{(l)} \left[\mathbf{y}^{(l)} - \mathbf{f}(\mathbf{x}^{(l)}) \right] \quad (4.3)$$

is minimized where

$$\mathbf{W}^{(l)} = \text{diag.} (w_1^{(l)}, w_2^{(l)}, \dots, w_n^{(l)}) \quad (4.4)$$

is the weighting factor for the l -th data point. Eq.(4.3) can be recast into

$$E = \sum_{l=1}^N \sum_{j=1}^n w_j^{(l)} \left[y_j^{(l)} - f_j(\mathbf{x}^{(l)}) \right]^2 = \sum_{j=1}^n \mathbf{r}_j^T \mathbf{W}_j \mathbf{r}_j \quad (4.5)$$

where

$$\mathbf{r}_j = \left[r_j^{(1)} r_j^{(2)} \dots r_j^{(N)} \right]^T \quad (4.6)$$

$$\mathbf{W}_j = \text{diag.} (w_j^{(1)}, w_j^{(2)}, \dots, w_j^{(N)}) \quad (4.7)$$

$$\begin{aligned} r_j^{(l)} &= f_j(\mathbf{x}^{(l)}) - y_j^{(l)} \\ &= a_j + \mathbf{b}_j^T \mathbf{x}^{(l)} + \sum_{i=1}^{\sigma} c_{ji} | \langle \alpha_i, \mathbf{x}^{(l)} \rangle - \beta_i | - y_j^{(l)} \end{aligned} \quad (4.8)$$

where a_j , and c_{ji} are the j -th components of the vectors \mathbf{a} and \mathbf{c}_i , respectively, and \mathbf{b}_j^T is the j -th row of the matrix \mathbf{B} . Let

$$\mathbf{z}_j = \left[a_j \ \mathbf{b}_j^T \ c_{j1} \ c_{j2} \ \dots \ c_{j\sigma} \right]^T \quad (4.9)$$

for $j=1,2,\dots,n$ and let

$$\mathbf{z}_{n+1} = \left[\alpha_1^T \ \alpha_2^T \ \dots \ \alpha_\sigma^T \ \beta_1 \ \beta_2 \ \dots \ \beta_\sigma \right]^T \quad (4.10)$$

then the approximation error is a function of these parameters; namely,

$$E = E(\mathbf{z}_1, \mathbf{z}_2, \dots, \mathbf{z}_n, \mathbf{z}_{n+1}) \quad (4.11)$$

and the optimal parameters $\mathbf{z}_1, \mathbf{z}_2, \dots, \mathbf{z}_n$ for the fixed partition $\mathbf{z}_{n+1} = \hat{\mathbf{z}}_{n+1}$ can be found by solving the equations

$$\frac{\partial E}{\partial \mathbf{z}_j} = 2 \mathbf{A} \mathbf{W}_j \mathbf{r}_j = 0 \quad (4.12)$$

for $i=1,2,\dots,n$, where

$$\mathbf{A} = \begin{bmatrix} 1 & 1 & \dots & 1 \\ x_1^{(1)} & x_1^{(2)} & \dots & x_1^{(N)} \\ x_2^{(1)} & x_2^{(2)} & \dots & x_2^{(N)} \\ \vdots & \vdots & \ddots & \vdots \\ x_n^{(1)} & x_n^{(2)} & \dots & x_n^{(N)} \\ u_1^{(1)} & u_1^{(2)} & \dots & u_1^{(N)} \\ u_2^{(1)} & u_2^{(2)} & \dots & u_2^{(N)} \\ \vdots & \vdots & \ddots & \vdots \\ u_\sigma^{(1)} & u_\sigma^{(2)} & \dots & u_\sigma^{(N)} \end{bmatrix} \quad (4.13)$$

$$u_i^{(l)} = | \langle \alpha_i, \mathbf{x}^{(l)} \rangle - \beta_i | \quad (4.14)$$

Since

$$\mathbf{r}_j = \mathbf{A}^T \mathbf{z}_j - \mathbf{y}_j \quad (4.15)$$

where

$$\mathbf{y}_j = \left[y_j^{(1)} \ y_j^{(2)} \ \dots \ y_j^{(N)} \right]^T \quad (4.16)$$

Equation (4.12) can be further reduced to

$$\mathbf{A} \mathbf{W}_j \mathbf{A}^T \mathbf{z}_j - \mathbf{A} \mathbf{W}_j \mathbf{y}_j = 0 \quad (4.17)$$

for $j=1,2,\dots,n$, and the optimal parameters \mathbf{z}_j^* for each j can be found efficiently via *parallel processing* by solving Eq.(4.17) for each j . In the special case where $\mathbf{W}_j = \mathbf{W}$ for every j , it becomes even more efficient since only a *single* Gaussian elimination is required for solving the n equations in Eq.(4.17).

We denote the solutions of Eq.(4.17) by $\mathbf{z}_j^*(\mathbf{z}_{n+1})$ for $j=1,2,\dots,n$, which are the optimal parameters in the canonical piecewise-linear equation (4.2) for the fixed partition \mathbf{z}_{n+1} . The next problem is to find the optimal partition boundaries \mathbf{z}_{n+1}^* such that

$$\begin{aligned} & E(\mathbf{z}_1^*(\mathbf{z}_{n+1}^*), \mathbf{z}_2^*(\mathbf{z}_{n+1}^*), \dots, \mathbf{z}_n^*(\mathbf{z}_{n+1}^*), \mathbf{z}_{n+1}^*) \\ & = \text{Min} \left\{ E(\mathbf{z}_1^*(\mathbf{z}_{n+1}), \mathbf{z}_2^*(\mathbf{z}_{n+1}), \dots, \mathbf{z}_n^*(\mathbf{z}_{n+1}), \mathbf{z}_{n+1}) \mid \mathbf{z}_{n+1} \in R^{n\sigma+\sigma} \right\} \end{aligned} \quad (4.18)$$

The procedures for searching the optimal partition \mathbf{z}_{n+1}^* are similar to those developed in Sections 2 and 3 for 2-terminal and 3-terminal devices. Let

$$\mathbf{g} = \frac{\partial E(\mathbf{z}_1, \mathbf{z}_2, \dots, \mathbf{z}_{n+1})}{\partial \mathbf{z}_{n+1}} = 2 \sum_{j=1}^n \mathbf{K}_j \mathbf{G} \mathbf{W}_j \mathbf{r}_j \quad (4.19)$$

where

$$\mathbf{K}_j = \text{diag.} (c_{j1}\mathbf{I}_n, c_{j2}\mathbf{I}_n, \dots, c_{j\sigma}\mathbf{I}_n, -c_{j1}, -c_{j2}, \dots, -c_{j\sigma}) \quad (4.20)$$

and \mathbf{I}_n is the n -dimensional identity matrix;

$$\mathbf{G} = \begin{bmatrix} \mathbf{XP}_1 \\ \mathbf{XP}_2 \\ \vdots \\ \mathbf{XP}_\sigma \\ \mathbf{P} \end{bmatrix}, \quad \mathbf{X} = \begin{bmatrix} x_1^{(1)} & x_1^{(2)} & \dots & x_1^{(N)} \\ x_2^{(1)} & x_2^{(2)} & \dots & x_2^{(N)} \\ \vdots & \vdots & \ddots & \vdots \\ x_n^{(1)} & x_n^{(2)} & \dots & x_n^{(N)} \end{bmatrix} \quad (4.21)$$

$$\mathbf{P}_i = \text{diag.} (p_i^{(1)}, p_i^{(2)}, \dots, p_i^{(N)}) \quad (4.22)$$

$$\mathbf{P} = \begin{bmatrix} p_1^{(1)} & p_1^{(2)} & \dots & p_1^{(N)} \\ p_2^{(1)} & p_2^{(2)} & \dots & p_2^{(N)} \\ \vdots & \vdots & \ddots & \vdots \\ p_n^{(1)} & p_n^{(2)} & \dots & p_n^{(N)} \end{bmatrix} \quad (4.23)$$

$$p_i^{(l)} = \text{sgn} (\langle \alpha_i, \mathbf{x}^{(l)} \rangle - \beta_i) \quad (4.24)$$

$$\mathbf{Y} = \frac{\partial \mathbf{g}}{\partial \mathbf{z}_{n+1}} = 2 \sum_{j=1}^n \left(\mathbf{K}_j \frac{\partial \mathbf{G}}{\partial \mathbf{z}_{n+1}} \mathbf{W}_j \mathbf{r}_j + \mathbf{K}_j \mathbf{G} \mathbf{W}_j \mathbf{G}^T \mathbf{K}_j^T \right) \quad (4.25)$$

The first term inside the summation of Eq.(4.25) can be eliminated since $\frac{\partial \mathbf{G}}{\partial \mathbf{z}_{n+1}} = 0$ almost everywhere except when the data points are coincident with the boundaries.

We then perform a line search along the direction

$$\mathbf{s} = -\mathbf{Y}^{-1}\mathbf{g} \quad (4.26)$$

as before until a local minimum is found. Since the current state of the art on global optimization[13,14] can not guarantee a global optimum, we simply repeat the same procedure with various partition boundaries until the error is within the acceptable tolerance. Otherwise, we must increase the number of partition boundaries.

5. Concluding Remarks

The canonical piecewise-linear model can be considered as a *universal* model in the sense that the form of the equations describing the model is the same for all device characteristics. Only the coefficients are different for different devices. It is this universal character which allows us to develop a highly efficient computational algorithm for solving dc nonlinear circuits.

Since our algorithm for determining the coefficients depends only on data extracted from the device's terminals, either by measurement or numerical methods, no knowledge of the internal device physics is required. This "black box" approach is particularly powerful in modeling dc characteristics of submicron and microwave devices where the internal device physics is not yet well understood.

Another advantage of the canonical piecewise-linear model is its small memory storage requirements. This advantage becomes decisive in large-scale circuits. To see this, let us compare the number of coefficients needed to specify an n -dimensional vector function $f: \mathbf{R}^n \rightarrow \mathbf{R}^n$, using the following three global representations :

1. *Canonical piecewise-linear representation* : Assuming that there are " k " $(n - 1)$ -dimensional boundary hyperplanes in each dimension, then Eq.(1.1) requires a total of $n^2 + n + nk(2n + 1) = O(n^2)$ coefficients.
2. *Conventional piecewise-linear representation* : Assume the domain space is partitioned into M regions, each described by an affine equation. Each region therefore requires $n^2 + n$ coefficients. Since M is generally a very large number especially when n is large, the storage requirement grows exponentially with n . To show this, consider the special case where the boundaries possess a lattice structure, and hence there are $(k + 1)^n$ regions in the domain space where " k " is as defined above. Hence the total number of coefficients is on the order of $O(n^2(k + 1)^n)$.
3. *n -variable polynomials of order m* : An m -th order polynomial in n variables requires $n(C(n, 0) + C(n, 1) + \dots + C(n, m))$ coefficients where $C(n, i) \equiv \frac{n!}{(n-i)! \times i!}$. For $n \gg m$, this is on the order of $O(n^m)$.

The above 3 estimates of memory requirements are plotted in Fig.12 for ease of comparison. Observe that the memory requirements for both the conventional piecewise-linear and the n -variable polynomial representations become excessive for large n . For example, when $n = 100$, $O(10^{80})$ and $O(10^{10})$ coefficients are required in the 2nd and 3rd representation for $k = 5$ and $m = 5$, respectively. Whereas only $O(10^4)$ coefficients are needed in the first representation. This comparison shows that the canonical piecewise-linear representation is currently the only practical global representation for high-dimensional vector-valued functions.

Appendix :

A. Canonical Piecewise-Linear Model for pn Junction Diode Characterized by Eq.(2.28)

3-segment model : Eq.(2.30)

4-segment model :

$$i = a + bv + c_1 |v - \beta_1| + c_2 |v - \beta_2| + c_3 |v - \beta_3| \quad (\text{A.1})$$

where

$$\begin{aligned} a &= -3.27 \times 10^{-2}, \quad b = 4.986 \times 10^{-2} \\ c_1 &= 2.955 \times 10^{-4}, \quad c_2 = 1.198 \times 10^{-2}, \quad c_3 = 3.758 \times 10^{-2} \\ \beta_1 &= 0.4612, \quad \beta_2 = 0.6216, \quad \beta_3 = 0.6684 \end{aligned}$$

5-segment model :

$$\begin{aligned} i &= a + bv + c_1 |v - \beta_1| + c_2 |v - \beta_2| + c_3 |v - \beta_3| \\ &+ c_4 |v - \beta_4| \end{aligned} \quad (\text{A.2})$$

where

$$\begin{aligned} a &= -3.9304 \times 10^{-2}, \quad b = 5.9581 \times 10^{-2}, \quad c_1 = 1.605 \times 10^{-4} \\ c_2 &= 5.555 \times 10^{-3}, \quad c_3 = 1.748 \times 10^{-2}, \quad c_4 = 3.624 \times 10^{-2} \\ \beta_1 &= 0.454, \quad \beta_2 = 0.6019, \quad \beta_3 = 0.6485, \quad \beta_4 = 0.6775 \end{aligned}$$

6-segment model :

$$\begin{aligned} i &= a + bv + c_1 |v - \beta_1| + c_2 |v - \beta_2| + c_3 |v - \beta_3| \\ &+ c_4 |v - \beta_4| + c_5 |v - \beta_5| \end{aligned} \quad (\text{A.3})$$

where

$$\begin{aligned} a &= -3.929 \times 10^{-2}, \quad b = 5.941 \times 10^{-2}, \quad c_1 = 8.915 \times 10^{-5}, \quad c_2 = 2.893 \times 10^{-3} \\ c_3 &= 8.838 \times 10^{-3}, \quad c_4 = 1.589 \times 10^{-2}, \quad c_5 = 3.170 \times 10^{-2}, \quad \beta_1 = 0.448 \\ \beta_2 &= 0.584, \quad \beta_3 = 0.632, \quad \beta_4 = 0.658, \quad \beta_5 = 0.679 \end{aligned}$$

7-segment model :

$$\begin{aligned} i &= a + bv + c_1 |v - \beta_1| + c_2 |v - \beta_2| + c_3 |v - \beta_3| \\ &+ c_4 |v - \beta_4| + c_5 |v - \beta_5| + c_6 |v - \beta_6| \end{aligned} \quad (\text{A.4})$$

where

$$\begin{aligned}
 a &= -4.660 \times 10^{-2}, \quad b = 6.997 \times 10^{-2}, \quad c_1 = 7.563 \times 10^{-5}, \quad c_2 = 2.335 \times 10^{-3} \\
 c_3 &= 7.032 \times 10^{-3}, \quad c_4 = 1.293 \times 10^{-2}, \quad c_5 = 2.107 \times 10^{-2}, \quad c_6 = 2.653 \times 10^{-2} \\
 \beta_1 &= 0.4468, \quad \beta_2 = 0.579, \quad \beta_3 = 0.626, \quad \beta_4 = 0.652 \\
 \beta_5 &= 0.672, \quad \beta_6 = 0.687
 \end{aligned}$$

B. Canonical Piecewise-Linear Bipolar Transistor Model

1. Optimized for Low Operating Voltages (less than 0.7V for each junction)

$$\begin{aligned}
 \begin{bmatrix} i_1 \\ i_2 \end{bmatrix} &= \begin{bmatrix} a_1 \\ a_2 \end{bmatrix} + \begin{bmatrix} b_{11} & b_{12} \\ b_{21} & b_{22} \end{bmatrix} \begin{bmatrix} v_1 \\ v_2 \end{bmatrix} + \begin{bmatrix} c_{11} \\ c_{21} \end{bmatrix} |v_1 - \beta_1| + \begin{bmatrix} c_{12} \\ c_{22} \end{bmatrix} |v_1 - \beta_2| \\
 &+ \begin{bmatrix} c_{13} \\ c_{23} \end{bmatrix} |v_1 - \beta_3| + \begin{bmatrix} c_{14} \\ c_{24} \end{bmatrix} |v_2 - \beta_4| + \begin{bmatrix} c_{15} \\ c_{25} \end{bmatrix} |v_2 - \beta_5| \\
 &+ \begin{bmatrix} c_{16} \\ c_{26} \end{bmatrix} |v_2 - \beta_6| \tag{B.1}
 \end{aligned}$$

where

$$\begin{aligned}
 \begin{bmatrix} a_1 \\ a_2 \end{bmatrix} &= \begin{bmatrix} -2.4604 \times 10^{-4} \\ -2.6340 \times 10^{-2} \end{bmatrix}, \quad \begin{bmatrix} b_{11} \\ b_{21} \end{bmatrix} = \begin{bmatrix} 4.083 \times 10^{-2} \\ -4.04167 \times 10^{-2} \end{bmatrix}, \quad \begin{bmatrix} b_{12} \\ b_{22} \end{bmatrix} = \begin{bmatrix} -4.04465 \times 10^{-2} \\ 8.0891 \times 10^{-2} \end{bmatrix} \\
 \begin{bmatrix} c_{11} \\ c_{21} \end{bmatrix} &= \begin{bmatrix} 2.461 \times 10^{-4} \\ -2.407 \times 10^{-4} \end{bmatrix}, \quad \begin{bmatrix} c_{12} \\ c_{22} \end{bmatrix} = \begin{bmatrix} 9.824 \times 10^{-3} \\ -9.726 \times 10^{-3} \end{bmatrix}, \quad \begin{bmatrix} c_{13} \\ c_{23} \end{bmatrix} = \begin{bmatrix} 3.076 \times 10^{-2} \\ -3.045 \times 10^{-2} \end{bmatrix} \\
 \begin{bmatrix} c_{14} \\ c_{24} \end{bmatrix} &= \begin{bmatrix} -2.405 \times 10^{-4} \\ 4.810 \times 10^{-4} \end{bmatrix}, \quad \begin{bmatrix} c_{15} \\ c_{25} \end{bmatrix} = \begin{bmatrix} -9.726 \times 10^{-3} \\ 1.945 \times 10^{-2} \end{bmatrix}, \quad \begin{bmatrix} c_{16} \\ c_{26} \end{bmatrix} = \begin{bmatrix} -3.048 \times 10^{-2} \\ 6.096 \times 10^{-2} \end{bmatrix} \\
 \beta_1 &= 0.4413, \quad \beta_2 = 0.6165, \quad \beta_3 = 0.6632 \\
 \beta_4 &= 0.4392, \quad \beta_5 = 0.6165, \quad \beta_6 = 0.6633
 \end{aligned}$$

2. Optimized for High Operating Voltages (up to 0.75V for each junction)

$$\begin{aligned}
 \begin{bmatrix} i_1 \\ i_2 \end{bmatrix} &= \begin{bmatrix} a_1 \\ a_2 \end{bmatrix} + \begin{bmatrix} b_{11} & b_{12} \\ b_{21} & b_{22} \end{bmatrix} \begin{bmatrix} v_1 \\ v_2 \end{bmatrix} + \begin{bmatrix} c_{11} \\ c_{21} \end{bmatrix} |v_1 - \beta_1| + \begin{bmatrix} c_{12} \\ c_{22} \end{bmatrix} |v_1 - \beta_2| \\
 &+ \begin{bmatrix} c_{13} \\ c_{23} \end{bmatrix} |v_1 - \beta_3| + \begin{bmatrix} c_{14} \\ c_{24} \end{bmatrix} |v_1 - \beta_4| + \begin{bmatrix} c_{15} \\ c_{25} \end{bmatrix} |v_2 - \beta_5| \\
 &+ \begin{bmatrix} c_{16} \\ c_{26} \end{bmatrix} |v_2 - \beta_6| + \begin{bmatrix} c_{17} \\ c_{27} \end{bmatrix} |v_2 - \beta_7| + \begin{bmatrix} c_{18} \\ c_{28} \end{bmatrix} |v_2 - \beta_8| \tag{B.2}
 \end{aligned}$$

where

$$\begin{bmatrix} a_1 \\ a_2 \end{bmatrix} = \begin{bmatrix} -1.840 \times 10^{-3} \\ -1.839 \times 10^{-1} \end{bmatrix}, \quad \begin{bmatrix} b_{11} \\ b_{21} \end{bmatrix} = \begin{bmatrix} 0.2654 \\ -0.2628 \end{bmatrix}, \quad \begin{bmatrix} b_{12} \\ b_{22} \end{bmatrix} = \begin{bmatrix} -0.2628 \\ 0.5256 \end{bmatrix}$$

$$\begin{bmatrix} c_{11} \\ c_{21} \end{bmatrix} = \begin{bmatrix} 1.115 \times 10^{-3} \\ -1.104 \times 10^{-3} \end{bmatrix}, \quad \begin{bmatrix} c_{12} \\ c_{22} \end{bmatrix} = \begin{bmatrix} 1.8786 \times 10^{-2} \\ -1.860 \times 10^{-2} \end{bmatrix}$$

$$\begin{bmatrix} c_{13} \\ c_{23} \end{bmatrix} = \begin{bmatrix} 6.885 \times 10^{-2} \\ -6.817 \times 10^{-2} \end{bmatrix}, \quad \begin{bmatrix} c_{14} \\ c_{24} \end{bmatrix} = \begin{bmatrix} 1.7668 \times 10^{-1} \\ -1.7493 \times 10^{-1} \end{bmatrix}$$

$$\begin{bmatrix} c_{15} \\ c_{25} \end{bmatrix} = \begin{bmatrix} -1.104 \times 10^{-3} \\ 2.208 \times 10^{-3} \end{bmatrix}, \quad \begin{bmatrix} c_{16} \\ c_{26} \end{bmatrix} = \begin{bmatrix} -1.860 \times 10^{-2} \\ 3.721 \times 10^{-2} \end{bmatrix}$$

$$\begin{bmatrix} c_{17} \\ c_{27} \end{bmatrix} = \begin{bmatrix} -6.817 \times 10^{-2} \\ 1.3634 \times 10^{-1} \end{bmatrix}, \quad \begin{bmatrix} c_{18} \\ c_{28} \end{bmatrix} = \begin{bmatrix} -1.749 \times 10^{-1} \\ 3.499 \times 10^{-1} \end{bmatrix}$$

$$\beta_1 = 0.5297, \beta_2 = 0.6362, \beta_3 = 0.6817, \beta_4 = 0.7144$$

$$\beta_5 = 0.5297, \beta_6 = 0.6362, \beta_7 = 0.6817, \beta_8 = 0.7144$$

References

- [1] J.L.Burns,A.R.Newton,and D.O.Pederson,"Active device table look-up models for circuit simulation," *Proc. 1983 Int. Symp. on Circuits and Systems* , May 1983, Newport Beach, California, pp. 250-253.
- [2] C. de Boor, *A Practical Guide to Splines* , New York : Springer-Verlag, 1978.
- [3] T.N.E. Greville, "Spline functions and applications," Lecture Note, University of Wisconsin, Madison, 1970.
- [4] S.M.Kang and L.O.Chua, "A global representation of multi-dimensional piecewise-linear functions with linear partitions," *IEEE Trans. Circuits and Systems* , Vol. CAS-25, pp.938-940, Nov. 1978.
- [5] M.Iri, "A method of multi-dimensional linear interpolation," (in Japanese), *J. Inform. Processing Soc. of Japan* , pp.211-215, July 1967.
- [6] T.E.Stern *Piecewise-linear network theory* , MIT Tech. Rep. 315, 1956.
- [7] T.Ohtsuki and N.Yoshida, "DC analysis of nonlinear networks based on generalized piecewise-linear characterization," *IEEE Trans. Circuit Theory* , CT-18, Jan. 1971, 146-151.
- [8] M.J.Chien and E.S.Kuh,"Solving nonlinear resistive networks using piecewise-linear analysis and simplicial subdivision," *IEEE Trans. Circuits and Systems* , CAS-24, Jan. 1977, 305-317.
- [9] L.O.Chua and R.Ying,"Canonical piecewise-linear analysis," *IEEE Trans. Circuits and Systems* , CAS-30, pp. 125-140, Mar. 1983.
- [10] L.O.Chua and A.C.Deng,"Canonical piecewise-linear analysis, Part II : tracing driving-point and transfer characteristics," *IEEE Trans. Circuits and Systems* , CAS-32, pp.417-445, May 1985.
- [11] L.O.Chua and A.C.Deng,"Canonical piecewise-linear analysis : generalized breakpoint hopping algorithm," *ERL Memo.* , UCB/ERL M85/36, University of California, Berkeley, Apr. 26, 1985.
- [12] G.W.Stewart, *Introduction to Matrix Computations* , New York : Academic Press, 1973.
- [13] L.Dixon and G.Szego, "The global optimization problem : an introduction," *Toward Global Optimization 2* , edited by L.Dixon and G.Szego, North-Holland Publishing Company, Amsterdam, Holland, pp.1-15, 1978.
- [14] W.Price, "Global optimization by controlled random search," *J. of Optimization Theory and Applications* , Vol. 40, No. 3, pp.333-348, July 1983.
- [15] J.J.Ebers and J.L.Moll, "Large signal behavior of junction transistors," *Proc. IRE* , Vol. 42, pp.1761-1772, Dec. 1954.
- [16] L.O.Chua and A.C.Deng,"Negative resistance devices; part II," *Int.J.Circuit Theory and Applications* , Vol.12, pp.337-373, Oct. 1984.
- [17] A.Ushida and L.O.Chua, "Tracing solution curves of nonlinear equation with sharp turning points," *Int.J. Circuit Theory and Applications* , Vol.12, pp.1-22, Jan. 1984.
- [18] H.Shichman and D.A.Hodges, "Modeling and simulation of insulated-gate field-effect transistor switching circuits," *IEEE J. Solid-State Circuits* , Vol. SC-3, pp.285-289, Sep. 1968.

- [19] T.Chen and M.S.Shur, "Analytical models of ion-implanted GaAs FET's,"
IEEE Trans. Electron Devices , VOL. ED-32, No.1, pp.18-28, Jan. 1985.

Figure Captions

- Fig.1 (a) Distribution of data points in Example 1; (b) approximation error *vs* the location of the breakpoint in Example 1.
- Fig.2 *v*-*i* characteristics predicted by two canonical piecewise-linear models for the pn junction diode : the 2-segment dashed curve is defined by Eq.(2.29); the 3-segment solid curve is defined by Eq.(2.30).
- Fig.3 2-port configuration of the bipolar transistor.
- Fig.4 (a) Boundary lines in Eq.(3.30) do not cover the whole "shaded" lower voltage region; (b) boundary lines $v_1 = E_1$ and $v_2 = E_2$ cover the whole "shaded" lower voltage region.
- Fig.5 (a) Three-dimensional plots for the emitter current in the Ebers-Moll model given by Eq.(3.27); (b) three-dimensional plot for the emitter current in the canonical piecewise-linear model given by Eq.(B.1) (low voltage version); (c) three-dimensional plot for the collector current in the Ebers-Moll model given by Eq.(3.27); (d) three-dimensional plot for the collector current in the canonical piecewise-linear model given by Eq.(B.1) (low voltage version); (e) comparison between the family of collector currents in the Ebers-Moll model (dashed line) and the canonical piecewise-linear model (solid line).
- Fig.6 (a) Odd-symmetric negative resistance circuit; (b) driving-point characteristic of the circuit in Fig.6(a).
- Fig.7 2-port configuration of the MOSFET.
- Fig.8 (a) Three-dimensional plot of drain current from the Shichman-Hodges model; (b) three-dimensional plot of the drain current from the canonical piecewise-linear model with a uniform weighting; (c) family of drain currents modeled by Eq.(3.39) (dashed line) and Eq.(3.43) (solid line); (d) three-dimensional plot of drain current in the canonical piecewise-linear model from Eq.(3.44) with a heavier weighting in the small v_{DS} region; (e) family of drain currents modeled by Eq.(3.39) (dashed line) and Eq.(3.44) (solid line).
- Fig.9 (a) NMOS inverter with depletion load; (b) $V_{out} - vs - V_{in}$ transfer characteristic of NMOS depletion load inverter.
- Fig.10 (a) CMOS inverter; (b) $V_{out} - vs - V_{in}$ transfer characteristic of CMOS inverter.
- Fig.11 Comparison of the canonical piecewise-linear model described by Eq.(3.46) (solid line) and the analytical model[19] (dashed line) for the ion-implanted GaAs FET.
- Fig.12 Comparison of memory storage requirement for a canonical piecewise-linear function (1), a conventional piecewise-linear function (2), and an *n*-variable polynomial (3) with order *m*.

Data points

x	y
0	0
1	1
2	1
3	0
4	-1
5	-1
6	1
7	2
8	-3
9	3
10	-2
11	3
12	1
13	2
14	3

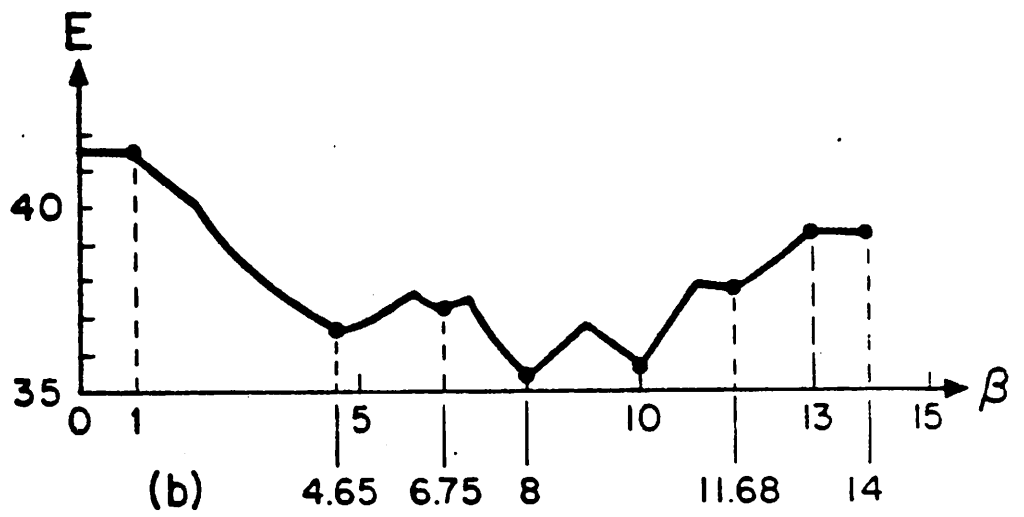
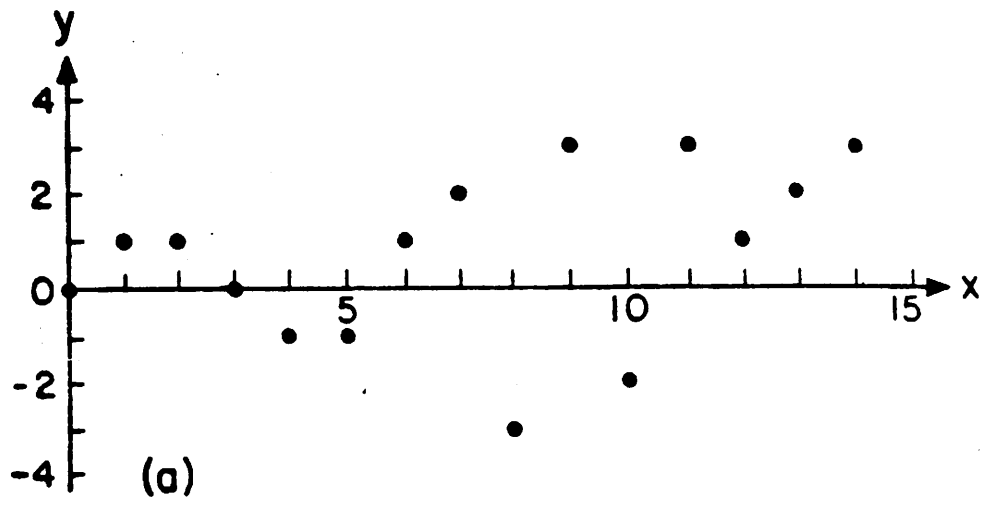


Fig. 1

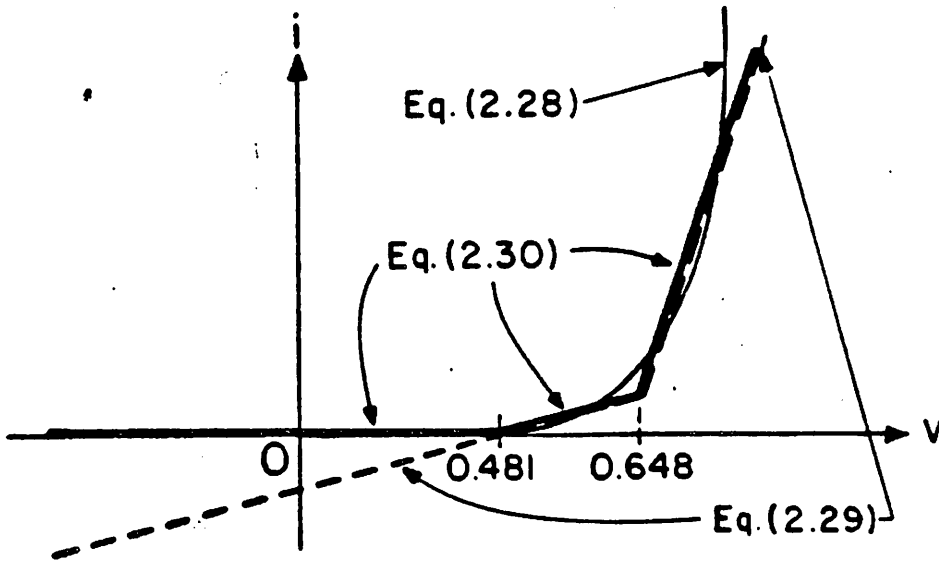


Fig. 2

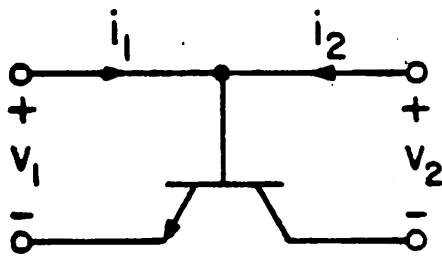


Fig. 3

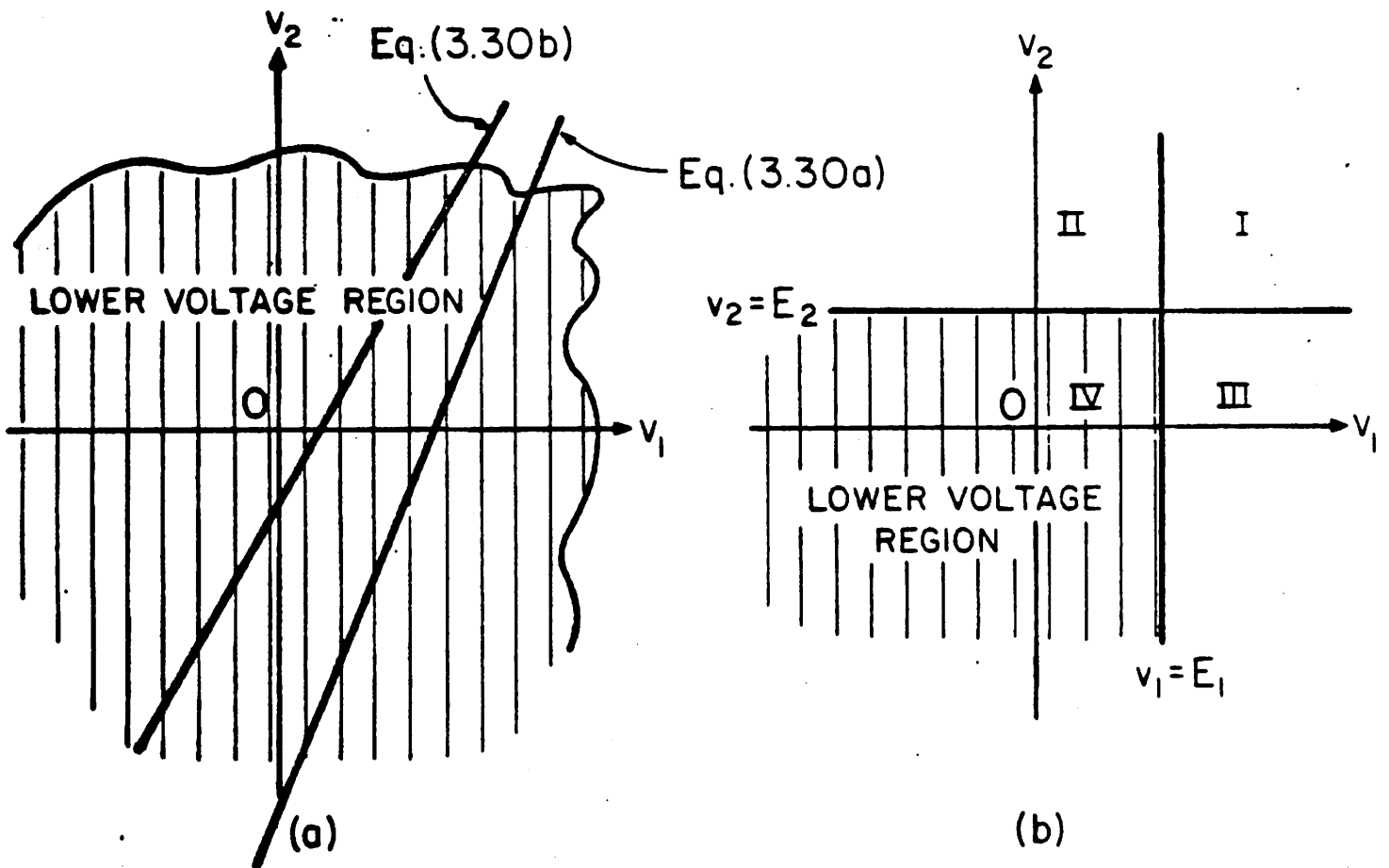
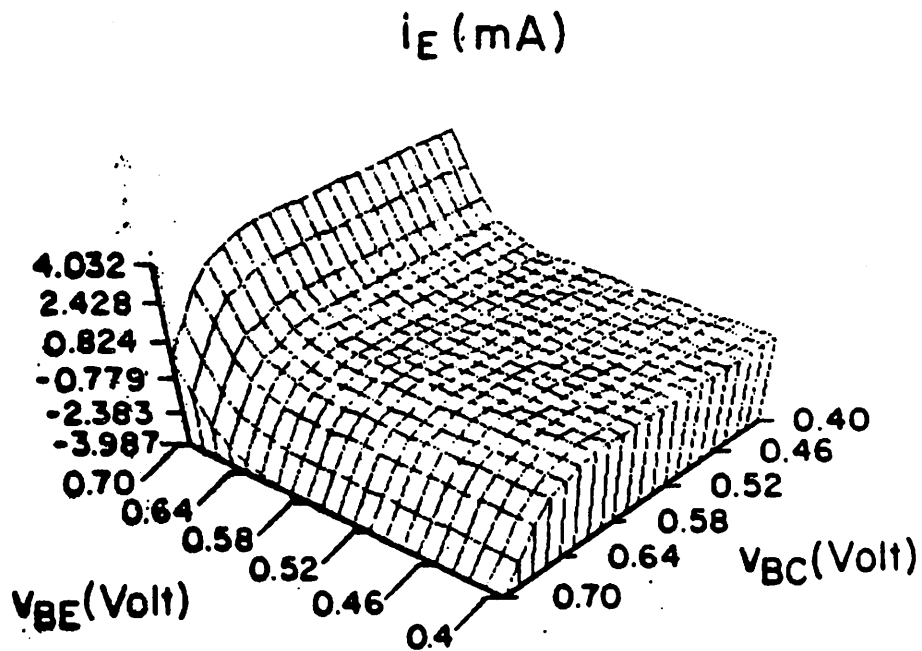
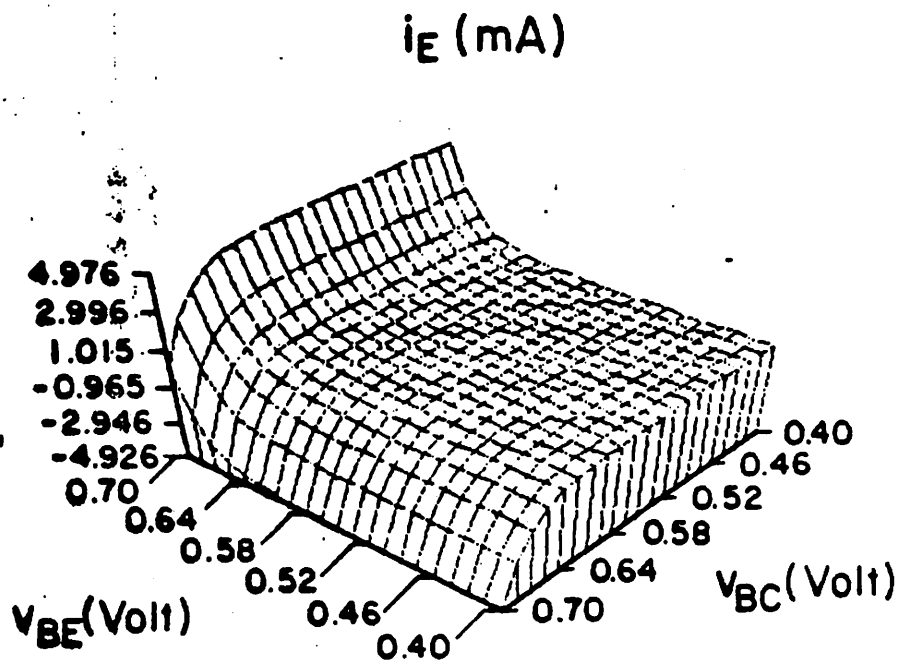


Fig. 4



i_c (mA)

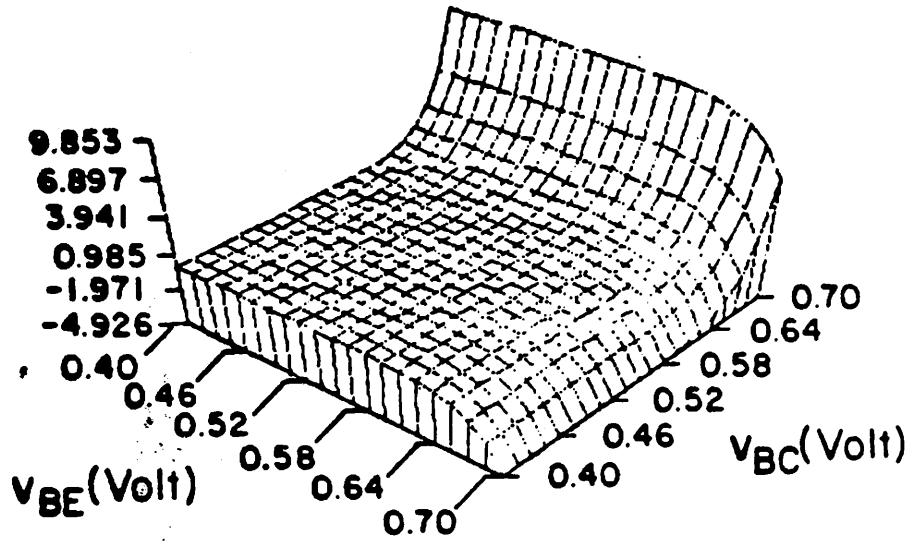


Fig. 5(c)

i_c (mA)

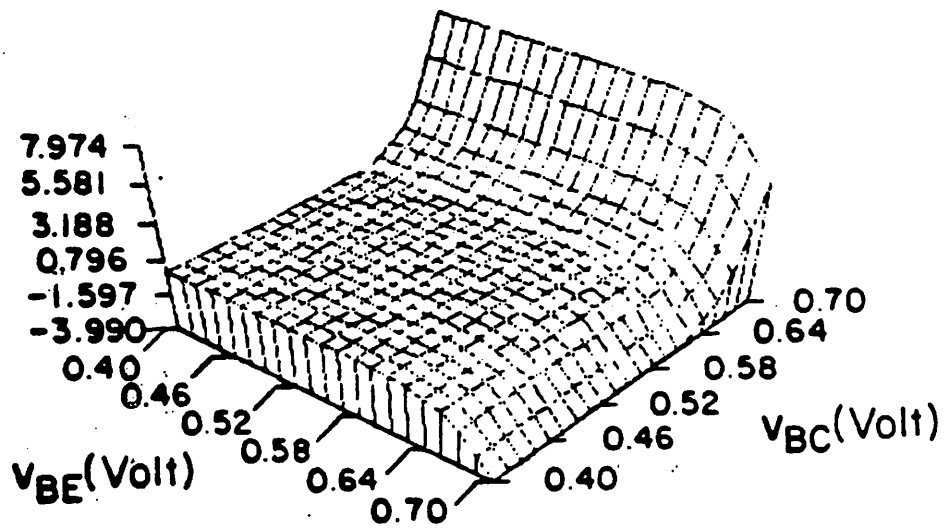


Fig. 5(d)

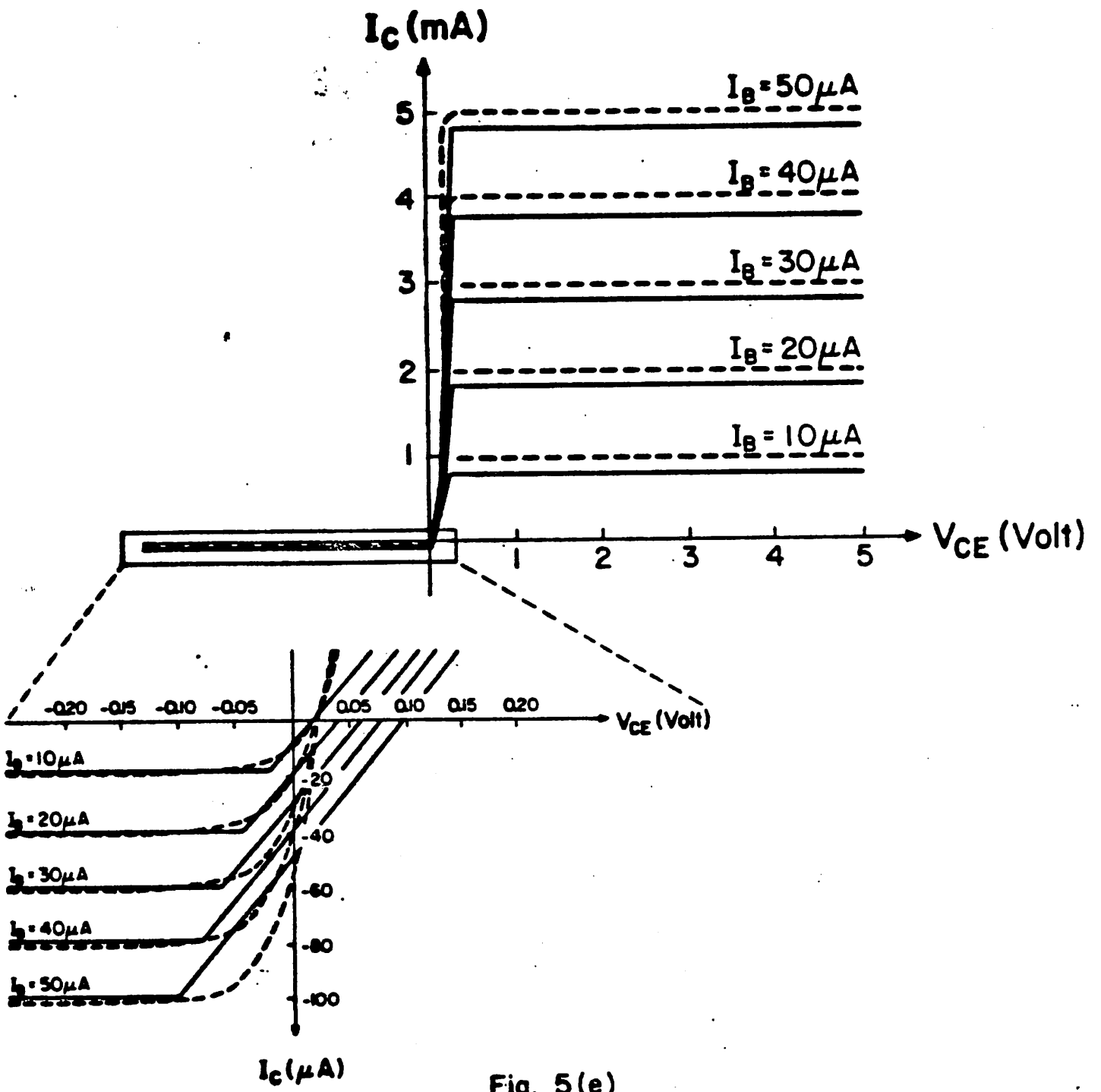
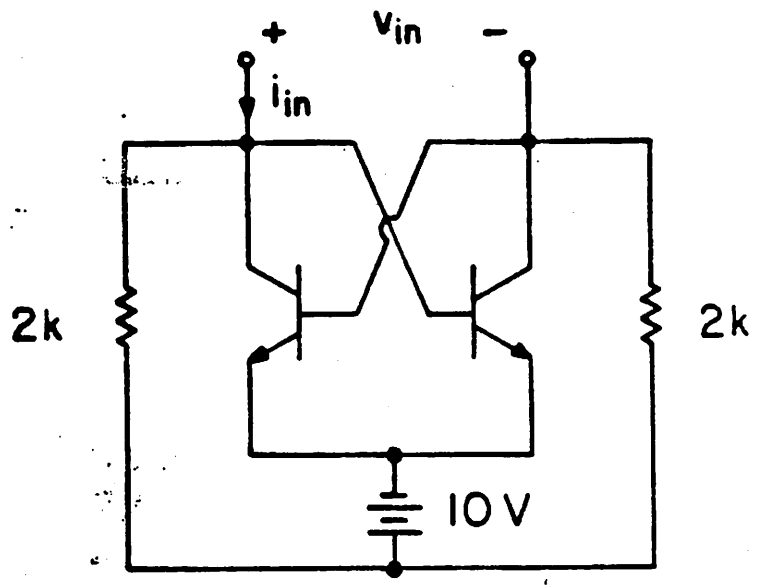
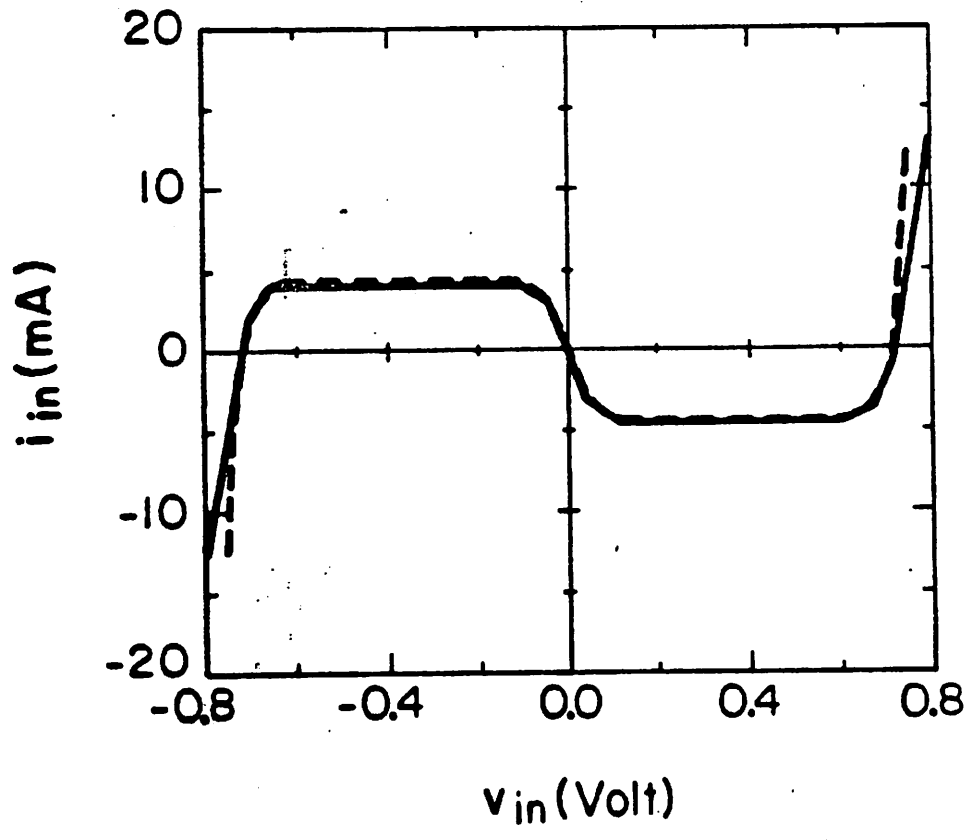


Fig. 5(e)



(a)

DP CHAR. OF ODD-SYMMETRIC CKT



(b)

Fig. 6

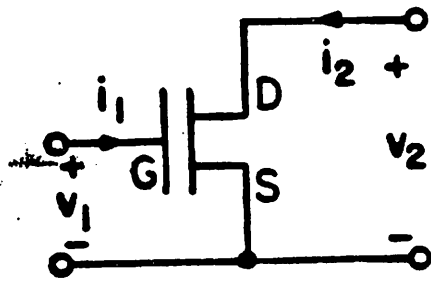


Fig. 7

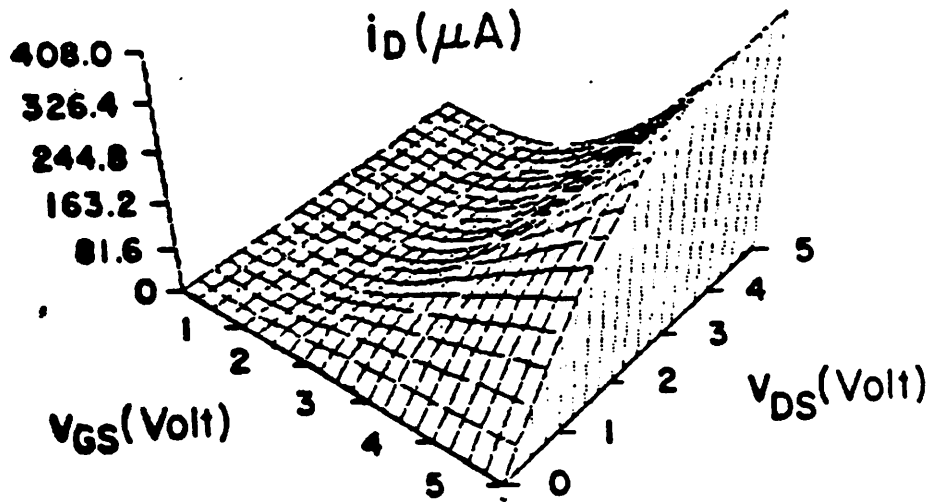


Fig. 8(a)

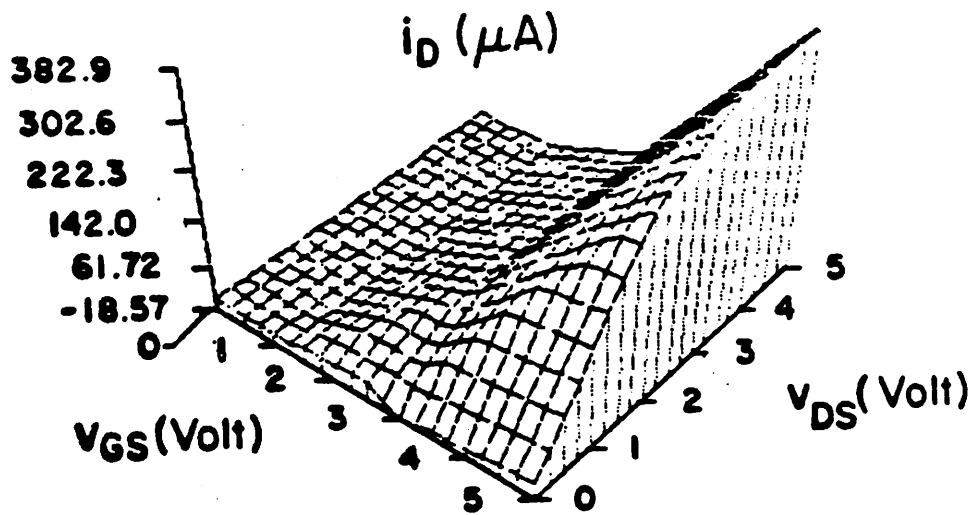


Fig. 8(b)

MOSFET OUTPUT CHAR.

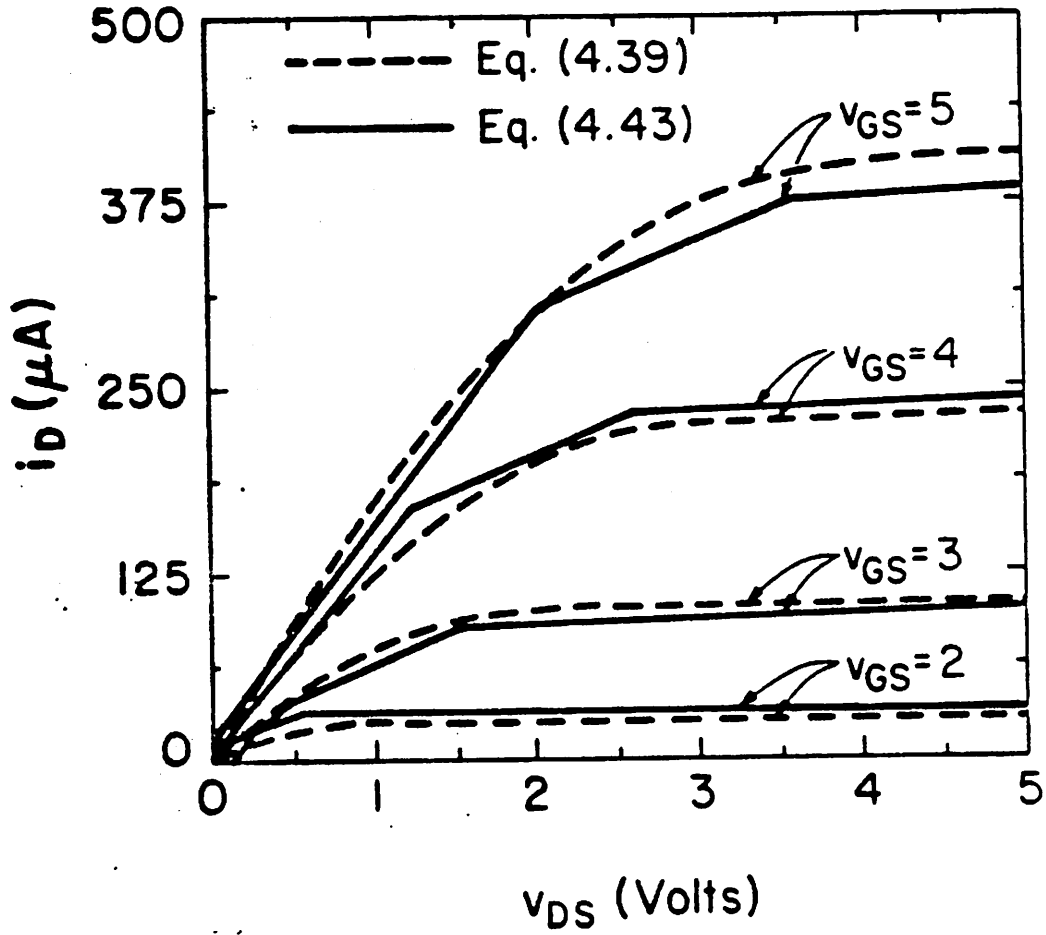


Fig. B(c)

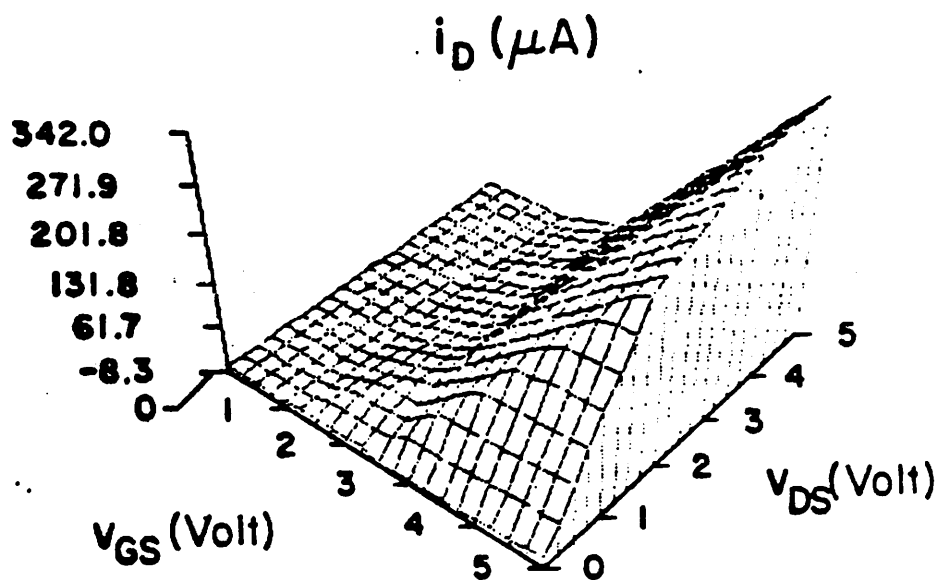


Fig. 8(d)

MOSFET OUTPUT CHAR.

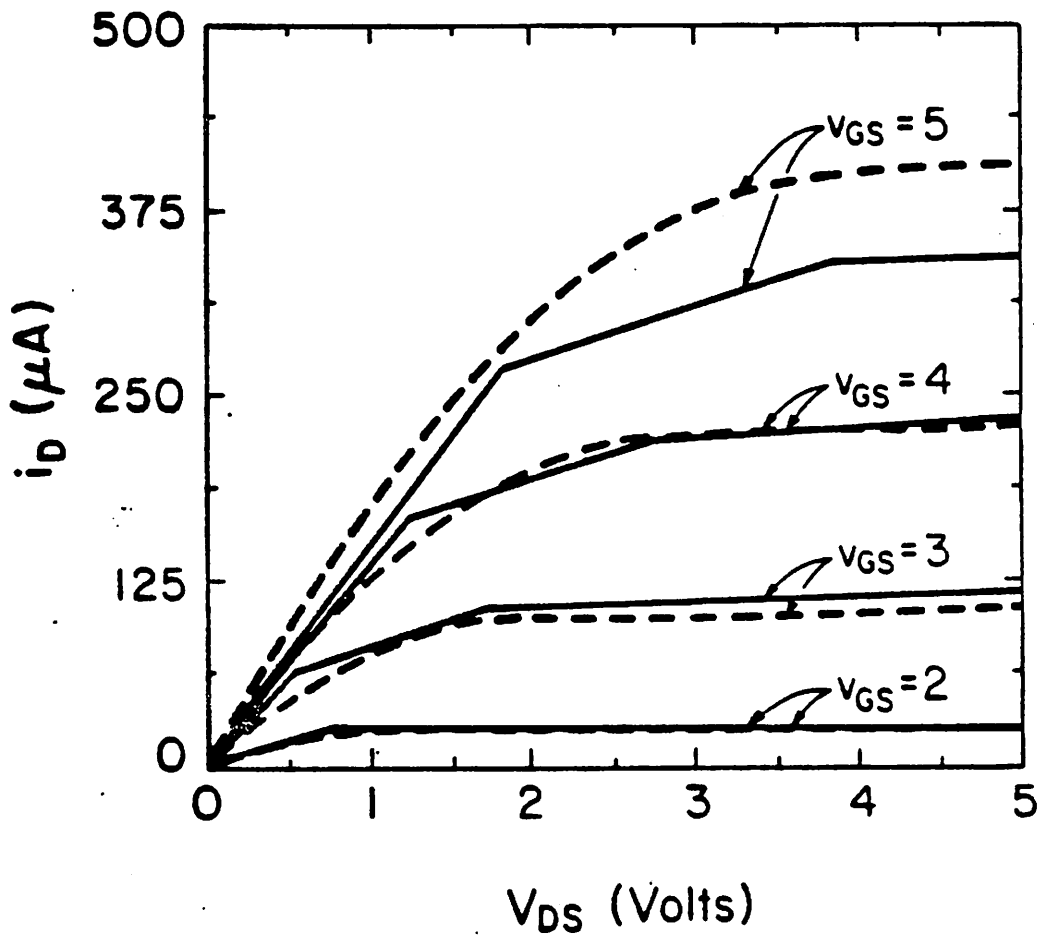
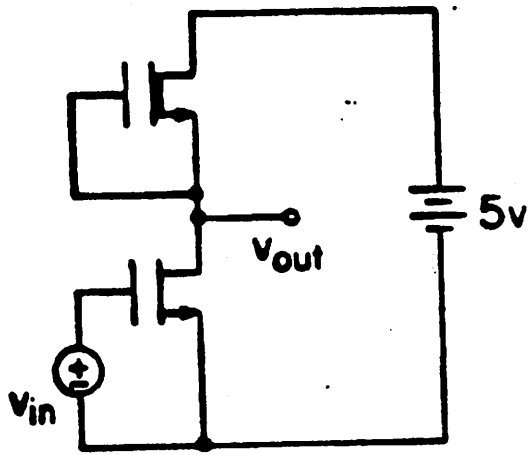
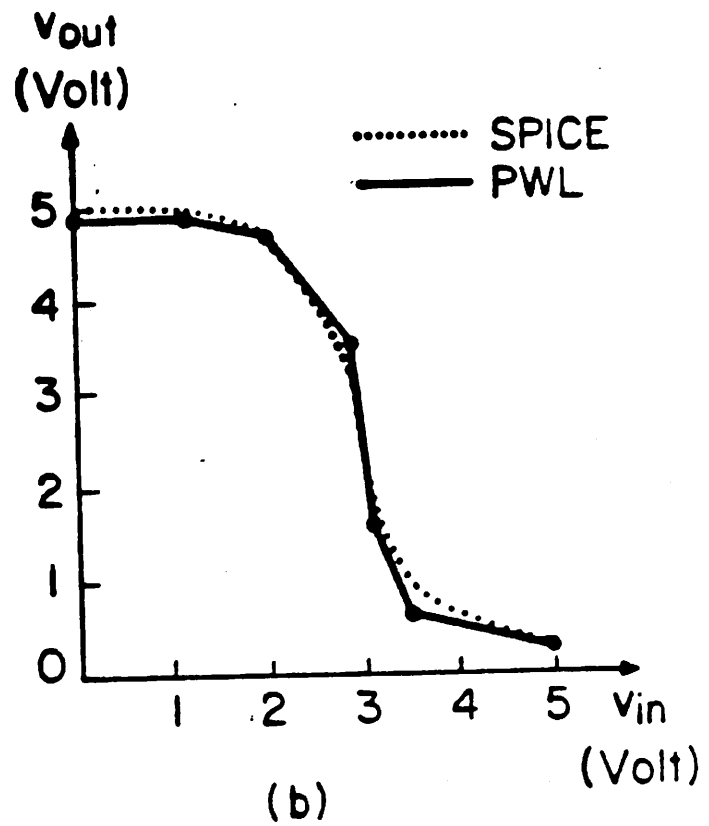


Fig. 8(e)

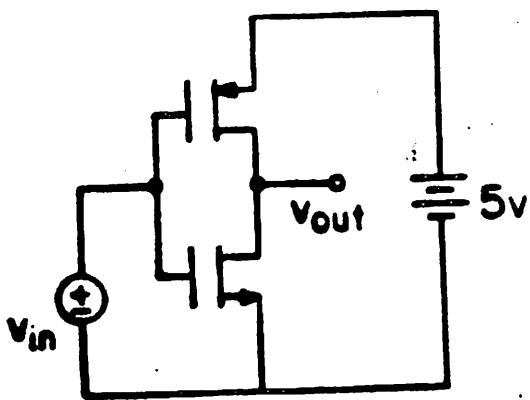


(a)

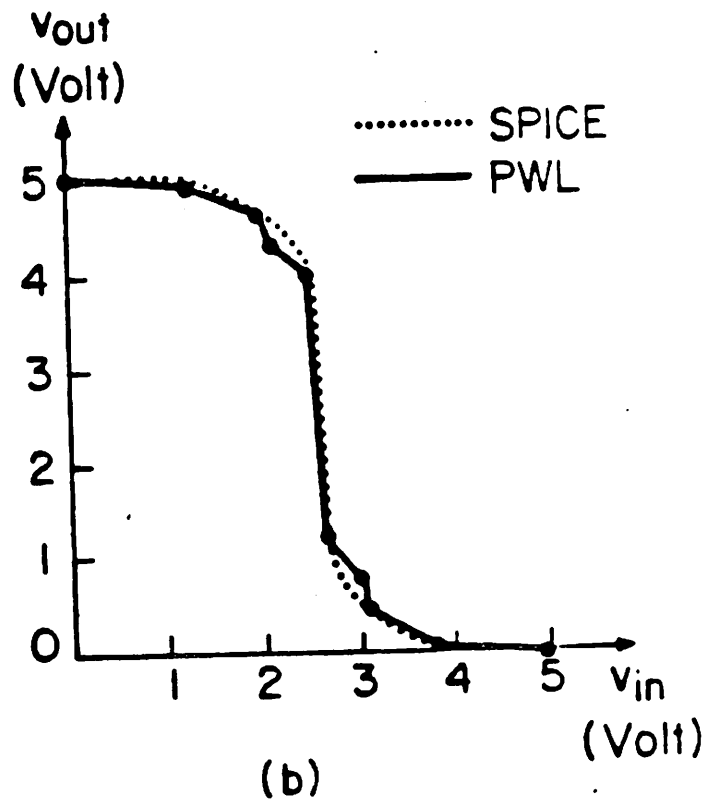


(b)

Fig. 9



(a)



(b)

Fig. 10

GaAs FET OUTPUT CHAR.

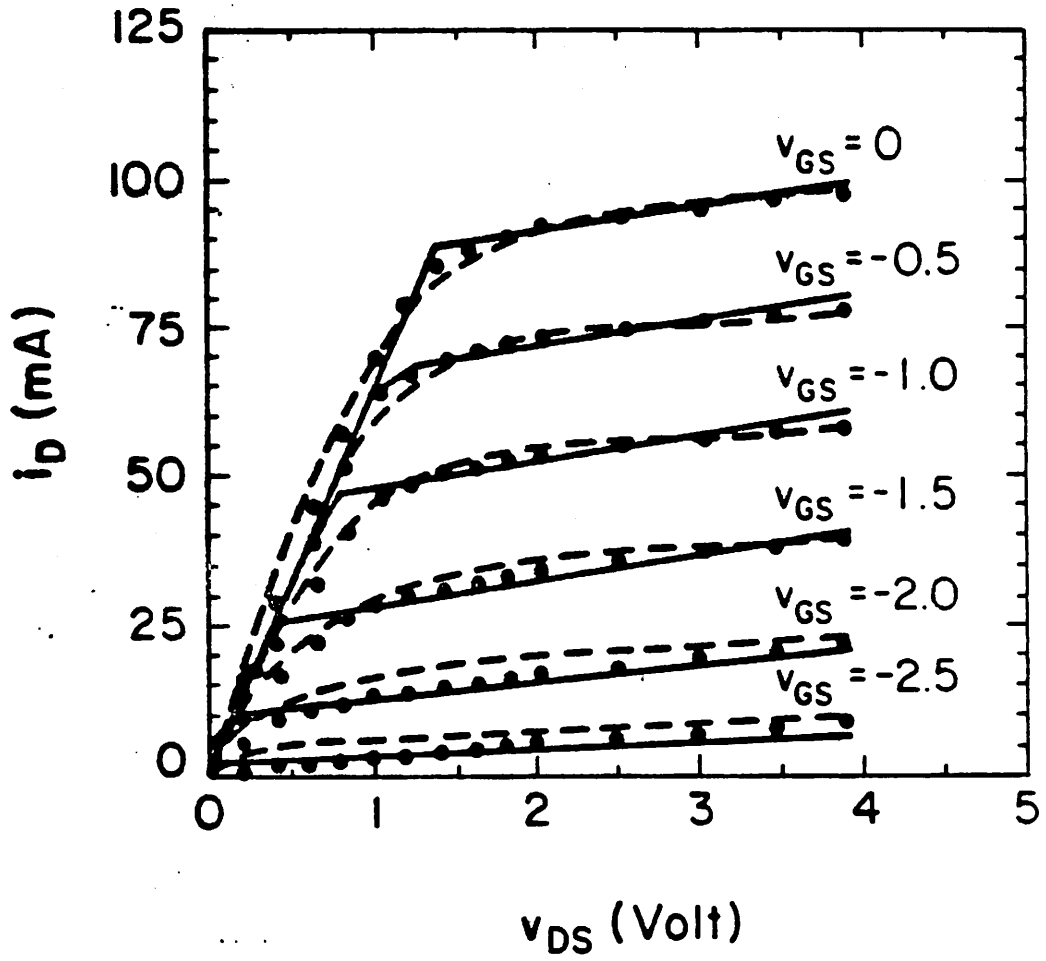
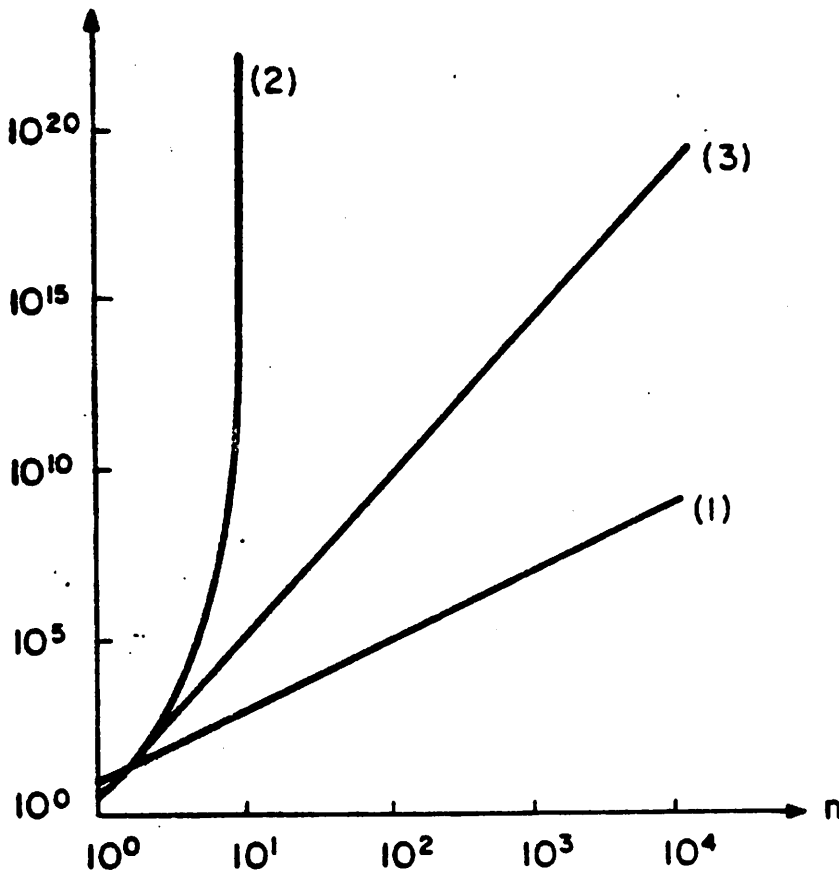


Fig. 11

N: Number of Parameters



1 : CANONICAL PWL ; $O(n^2)$

2 : GENERAL PWL ; $O[n^2(k+1)^n]$

3 : n-variable POLYNOMIAL of order m ; $O(n^m)$

Fig. 12